The Thesis Committee for Yangchuan Li
Certifies that this is the approved version of the following thesis:

Ab initio Study of Carbon Nanotube Based Conductors

APPROVED BY
SUPERVISING COMMITTEE:

Supervisor:

Eric Fahrenthold

Eric Taleff

Ab initio Study of Carbon Nanotube Based Conductors

by

Yangchuan Li, B.E.

Thesis

Presented to the Faculty of the Graduate School of

The University of Texas at Austin

in Partial Fulfillment

of the Requirements

for the Degree of

Master of Science in Engineering

The University of Texas at Austin

May 2017

Acknowledgements

My deep gratitude goes first to Dr. Eric Fahrenthold for his invaluable supports and expert insights during my research. I would also like to express appreciation to my family who always gives the best as they can to help me.

This work was supported by the Office of Naval Research (Grant N00014-15-1-2693). Computer time support was provided by the Texas Advanced Computing Center at the University of Texas at Austin.

Abstract

Ab initio Study of Carbon Nanotube Based Conductors

Yangchuan Li, M.S.E.

The University of Texas at Austin, 2017

Supervisor: Eric Fahrenthold

The development of new high strength, high reliability, and high ampacity conductors can benefit a wide range of commercial and military systems. Improved conductors are needed to perform a variety of power and data transmission functions, and their strategic research importance is highlighted in numerous publications. The most promising opportunities for fundamental improvements in conductors appear to be offered by carbon nanotube (CNT) based composites. Material architectures of interest include doped nanotube wires and cables, and nanotube-copper composites. Although the electrical conductivity of current CNT fibers lag copper by an order of magnitude, a mass specific comparison shows that CNT composites are promising candidates for disruptive advances in conductor technology. The majority of published research on carbon nanocomposite conductors has taken an experimental approach. Although experimental research has been productive, the complexity of the materials design problem motivates complementary efforts on simulation. Simulation can serve as a valuable adjunct to experiment, in particular when published experimental studies speculate on physics which may not be amenable to direct experimental measurement.

This thesis investigates the conductance of iodine or chromium doped CNT and copper-CNT nanocomposites using ab initio methods, which can complement experimental work by estimating the performance of systems that may be difficult to study experimentally. Both conductor and junction models of these nanomaterials were built to perform conductance calculations. Based on the computed microscopic properties, a transmission line model is proposed to predict the behavior of nanowires. The results suggest that iodine doped carbon nanotube conductors are viable research and development candidates for electrical conductors in ship and aircraft applications, where mass specific conductivity is of central interest.

Table of Contents

List of Tables viii

List of Figures ix

Chapter 1: Introduction 1

1.1 Carbon Nanotube Based Conductors 1

1.2 Ballistic Conductance Analysis 3

1.3 Previous Work on Ballistic Conductance Analysis 5

1.4 Outline of Thesis 6

Chapter 2: Iodine Doped CNT 8

2.1 Introduction 8

2.2 Modeling Configuration 9

2.3 Results and Discussion 10

2.3.1 Iodine Doped CNT Conductors 10

2.3.2 Iodine Doped CNT Junctions 12

2.4 Conclusions 14

Chapter 3: Double Wall Carbon and Copper Tubes 16

3.1 Introduction 16

3.2 Modeling Configuration 16

3.2.1 Modeling Constraints 18

3.2.2 Double Wall Tube with Metallic CNT and Copper 18

3.2.3 Double Wall Tube with Semiconducting CNT and Copper 20

3.2.4 Double Wall CNT 21

3.2.5 Junction Alignment 23

3.3 Results and Discussion 24

3.3.1 Scaled Conductance and Scaled Specific Conductance 24

3.3.2 Double Wall Tube with Copper and CNT 24

3.3.3 Double Wall CNT 27

3.4 Conclusions 30

Chapter 4: Polyiodide Doped CNT 32
4.1 Introduction 32
4.2 Modeling Configuration 32
4.3 Results and Discussion 34
4.3.1 Polyiodide Doped CNT Conductors 35
4.3.2 Polyiodide Doped CNT Junctions 39
4.4 Conclusions 42
Chapter 5: Transmission Line Model 43
5.1 Introduction 43
5.2 Consistency Check 44
5.3 Results and Discussion 45
5.3.1 Double Wall Tube with Copper and CNT 45
5.3.2 Polyiodide doped CNT 47
Chapter 6: Conclusions 50
6.1 Double Wall Carbon and Copper Tubes 50
6.2 Polyiodide Doped CNT 52
6.3 Thesis Contributions 52
References 55

List of Tables

Table 1.1: Electrical conductivity of alternative materials 3

Table 1.2: Mass specific electrical conductivity of alternative materials 3

Table 3.1: Dimensions of the cells used to model the DWCNT.....22

Table 5.1: Computational predictions of copper-CNT model in transmission line model.....46

Table 5.2: High performance combinations of iodine doped CNT.....48

List of Figures

Figure 1.1: Naming of CNT (Adapted from reference [6])....1

Figure 2.1: CNT(5, 5) calculation model 10

Figure 2.2: Conductance results for CNT(5, 5)....10

Figure 2.3: Iodine doped CNT models....11

Figure 2.4: CNT conductance versus applied dopant....11

Figure 2.5: CNT junction model dimensions 12

Figure 2.6: Junction model at different overlaps....13

Figure 2.7: Aligned (left) and misaligned (right) configurations....13

Figure 2.8: Junction conductance versus overlap....14

Figure 3.1: Band structure of CNT(9, 0) and CNT(5, 5)....17

Figure 3.2: Dimension of the CNT(M)@Cu model 19

Figure 3.3: Dimensions of the CNT(M)@Cu (left) and Cu@CNT(M) (right) doped junctions....20

Figure 3.4: Dimensions of the CNT(S)@Cu model....20

Figure 3.5: Dimension of the CNT(S)@Cu (left) and Cu@CNT(S) (right) doped junctions....21

Figure 3.6: Double wall CNT (left) with CNT(5, 5)@CNT(10, 10) (naming convention is inner@outer), commensurate arrangement (center) and incommensurate arrangement (right) (Adapted from reference [67])21

Figure 3.7: CNT(5,5)@CNT(18,0) (left) and CNT(9,0)@CNT(10,10) (right)...22

Figure 3.8: CNT-CNT junction (left) and copper-copper junction (right)....23

Figure 3.9: Conductor, undoped junction and doped junction for the Cu@Cu models 25

Figure 3.10: Conductor, undoped junction, and doped junction for the CNT(M)@Cu models 25
Figure 3.11: Conductor, undoped junction, and doped junction for the Cu@CNT(M) models 26
Figure 3.12: Conductance and specific conductance: copper and metallic CNT models 26
Figure 3.13: Conductance and specific conductance: copper and semiconducting CNT models 27
Figure 3.14: Conductor, undoped junction and doped junction for CNT(M)@CNT(M) 28
Figure 3.15: Conductance and specific conductance: commensurate CNT models (both CNT's metallic or both semiconducting) 28
Figure 3.16: Conductance and specific conductance: incommensurate CNT Models (one metallic CNT, one semiconducting CNT) 29
Figure 3.17: Specific conductance of the double wall models 30
Figure 3.18: Conductance of the various junction models 31
Figure 4.1: CNT(5, 5) (left) and CNT(8, 0) (right) 33
Figure 4.2: Metallic CNT(5, 5) model with aligned 0.7 iodine/unit cell (left), aligned 1.0 iodine/unit cell (center), random 2.3 iodine/unit cell (right) 35
Figure 4.3: Conductance for the metallic CNT models 35
Figure 4.4: Semiconducting CNT(8, 0) model with aligned 1.0 iodine/unit cell (left), aligned 1.5 iodine/unit cell (middle), random 4.9 iodine/unit cell (right) 36
Figure 4.5: Conductance for the semiconducting CNT models 37

Figure 4.6: Interstitially doped metallic CNT(5, 5) with unrelaxed 1.3 iodine/unit cell (left), relaxed 1.3 iodine/unit cell (center), relaxed 2.0 iodine/unit cell (right).....37
Figure 4.7: Conductance of interstitially doped two CNT(5, 5).....38
Figure 4.8: Interstitial doped semiconducting CNT(8, 0) with unrelaxed 2.0 iodine/unit cell (left), relaxed 2.0 iodine/unit cell (middle), relaxed 3.0 iodine/unit cell (right) 38
Figure 4.9: Conductance of interstitially doped dual CNT(8, 0).....39
Figure 4.10: Doped metallic CNT(5, 5) junction with overlap equals to 2 unit cells (left) and 10 unit cells (right).....40
Figure 4.11: Conductance of metallic CNT(5, 5) junction.....40
Figure 4.12: Doped CNT(8, 0) junction with overlap equals to 0.7 unit cells (left) and 4.7 unit cells (right).....41
Figure 4.13: Conductance of semiconducting CNT(8, 0) junction 41
Figure 5.1: Transmission line model.....43
Figure 5.2: Performance evaluation for the copper-CNT nanowires 45
Figure 5.3: Performance evaluation on CNT-CNT nanowires.....47
Figure 5.4: Performance evaluation on iodine doped CNT system.....49
Figure 6.1: Relative performance of double wall tube systems (For copper-CNT $Lm = 50nm$, for CNT-CNT $Lm = 100nm$, for all $n = 1$) 50

Chapter 1: Introduction

1.1 Carbon Nanotube Based Conductors

The widespread use of copper in power and data cabling for aircraft, ships, and ground vehicles imposes significant mass penalties and can limit system performance. Carbon nanotube (CNT) [1], [2] based electrical conductors have attracted considerable attention, as potential replacements for copper, since they may offer improved specific conductivity [3] and higher ampacity [4], [5].

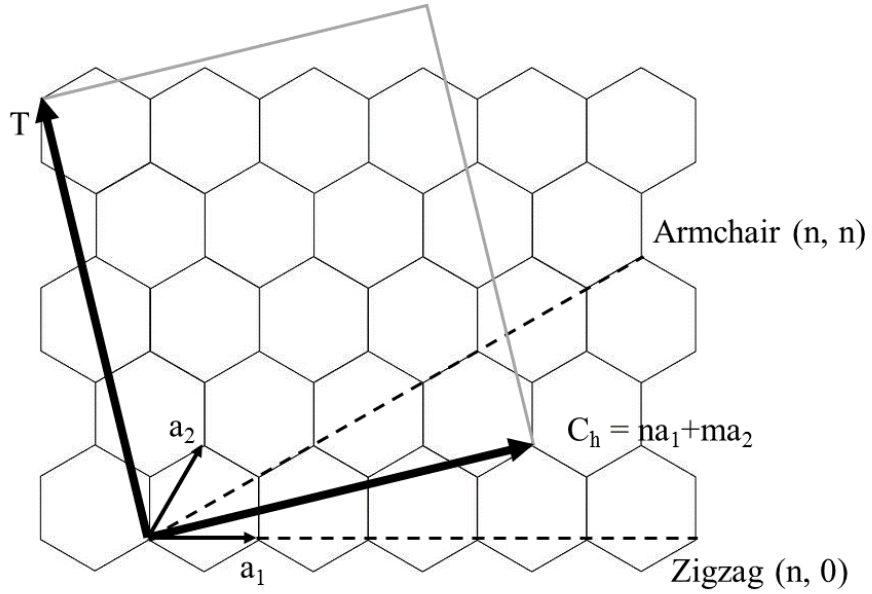

Figure 1.1: Naming of CNT (Adapted from reference [6])

A CNT is an allotrope of carbon, with a cylindrical structure. Since its first discovery [7], many research publications have revealed that it has fascinating mechanical [8], electrical [9]–[11] and thermal [12], [13] properties. The structure of a CNT is described by a chirality index (n, m), which defines the wrapping angle and diameter of the CNT. When $n = m$, the CNT is called armchair CNT. When $m = 0$, the CNT is named zigzag. In Figure 1.1, a_1 and a_2 are the unit vectors of graphene. C_h denotes the chiral

vector. A CNT can be viewed as rolled up platelet of graphene, the latter defined by the C_h vector. The diameter of a CNT is equal to the length of C_h. T denotes the tube axis.

Chirality determines the electrical properties of a CNT. Generally speaking, when $n - m = 3t$ ($t = 0, 1, 2 \ldots$), the CNT will be metallic [14], e.g. CNT(5, 5). Otherwise, it is semiconducting, e.g. CNT(8, 0). In some cases, e.g. CNT(9, 0), a CNT categorized as metallic actually has a small bandgap, as shown by Blase et al. [15].

CNT based conductors have been studied both experimentally and computationally, as a promising new cable technology. Their relatively low conductivity [16], as compared to copper, has encouraged the consideration of doped nanotubes or CNT-copper nanocomposites as energy efficient replacements in mass sensitive applications. Table 1.1 and Table 1.2 compare published data on the electrical conductivity and the mass specific electrical conductivity of several doped CNT or CNT-based composites with the corresponding properties of copper.

Although experimental research on the development of CNT based electrical conductors has been productive, the difficulty of the conductor design problem motivates complimentary computational research. This thesis contributes additional studies on iodine doped CNT cables and copper-CNT nanomaterials. Specifically, it includes a series of ab initio calculations performed to estimate the ballistic conductance properties of iodine doped carbon nanotubes and copper-CNT nanomaterials, which are under consideration as potential replacements for copper in ship and aircraft applications. Such applications are typically mass constrained, as opposed to volume constrained, hence specific conductivity (as opposed to conductivity) is of most interest. Since the fabrication of macroscale conductors will presumably require the systematic integration of nanotube bundles, the conductance properties of both nanotube conductors and nanotube junctions, including both doped and undoped models, are investigated.

Material	Conductivity $\sigma\ (S/cm)$
Cu	5.80×10^5 [4]
Cu-CNT composite	$(2.3 - 4.7) \times 10^5$ [4]
Undoped CNT fiber	$(1.82 - 2.90) \times 10^4$ [17], [18]
Iodine doped CNT fiber	$(5.00 - 6.67) \times 10^4$ [3], [17]
Acid doped CNT fiber	$(2.42 - 3.89) \times 10^4$ [5]

Table 1.1: Electrical conductivity of alternative materials

Material	Specific conductivity $\sigma/\rho\ (S \cdot cm^2/g)$
Cu	6.47×10^4 [4]
Cu-CNT composite	8.15×10^4 [4]
Iodine doped CNT fiber	1.96×10^5 (best) [3]

Table 1.2: Mass specific electrical conductivity of alternative materials

1.2 Ballistic Conductance Analysis

The computational package used in this thesis is the open source code SIESTA [19], which based on density functional theory (DFT) and employs atomic orbitals as a basis set. The electrical transport properties are computed using a non-equilibrium Green's

function (NEGF) formalism [20], implemented in the TranSIESTA module [21] of the SIESTA package. First SIESTA is used to determine the electronic structure, then TranSIESTA is used to compute the modeled system's electrical conductance.

As described in the TranSIESTA documentation [21], some modeling assumptions should be noted:

- Ballistic transport is assumed. So the mean free path L_m of an electron is assumed to be greater than the length of the conductor L_c. For single-walled CNT at room temperature, L_m is estimated to fall within the range 10-4,000 nm [22], [23].
- Zero temperature conditions are assumed, in the molecular sense, since the electronic structure calculations are performed for fixed nuclei (Born-Oppenheimer approximation).

The electrical conductance (G) is calculated using the Landauer formula [24].

$$G = 2\frac{e^2}{h}\int -\frac{\partial f(E)}{\partial E}T(E)dE\,, \qquad T(E) = Tr[t^*(E)t(E)]$$

Here e is the electron charge, h is Planck's constant, $f(E)$ is the Fermi-Dirac distribution function, $T(E)$ is the transmission function and $t(E)$ is a matrix of transmission coefficients for waves propagating along the conductor. Note that E is the wave energy. To obtain the conductance at ground state, let

$$-\frac{\partial f(E)}{\partial E} = \delta(E - E_f)$$

where E_f is the Fermi energy, so that

$$G = G_0 T(E_f), \quad G_0 = 2\frac{e^2}{h} = 7.75 \times 10^{-5}\ \mathrm{S}$$

Here G_0 is the standard quantum conductance unit. For an ideal metallic carbon nanotube, $T(E_f) = 2$ and $G = 2G_0$ [25].

1.3 Previous Work on Ballistic Conductance Analysis

The most widely used approach to ballistic conductance modeling employs density functional theory and a non-equilibrium Green's function formulism to studying electron transport properties of nanoscale conductors [26]–[28]. Based on this approach, extensive ballistic conductance analyses on various CNT systems has been performed. Since a macroscopic CNT cable is composed of many nanoscale CNT conductors and junctions, modeling work on the ballistic conductance of both CNT conductors and junction is of major interest.

Analytical work on CNT conductors has included: (1) introducing defects (e.g. vacancies [29]), (2) applying chemical doping (e.g. F [30], I_2, ICl, IBr [31], MoO_3 [32], AuCl3 [33]), (3) building multiwall CNT models (e.g. double CNT in which each tube has different electrical properties [34] or double wall CNT with variation in interwall spacing [35]), and (4) investigating nanocomposite nanowires (e.g. Cu-CNT conductors [36] and sulfur chains positioned inside CNT [37]). Some research has combined more than one configuration parameter. For example, Lopez-Bezanilla [38] investigated chemically doped double wall CNT, examining the effects of both interwall spacing and outer wall modification [by monovalent phenyl ($-C_6H_5$) and divalent dichlorocarbene ($>CCl_2$) dopants] on conductor performance. The results suggested that monovalent dopants have stronger negative effects on conductance than divalent dopants. They noted that large interwall spacing prevent the negative effects of outer tube doping from affecting inner tube.

In the case of CNT junctions, modeling research has focused on: (1) structural effects (e.g. variations in junction overlap [39], [40] or tube angles [41], [42]), and (2) the effects of chemical doping on junction performance (including transition metals [43], gold nanoparticles [44], or O_2 and N_2 [45]). The computational results indicate that the

conductance ‘oscillates’ with junction overlap, which may explained by ‘quantum interference’ effects [39], [40]. In term of tube angles, the highest conductance is found when the junction region structure is ‘commensurate’ [42]. In the case of transition metal doping, it appears that the best junction conductance results from chromium doping [43].

In the case of CNT network modeling, most modeling work has employed percolation theory which incorporates both conductor and junction performance. As an example, computational work described in references [46], [47], combines the macroscopic conductor performance with the ballistic conductance of the junctions to predict the performance of CNT composites. In this thesis, overall CNT network performance is estimated by developing a transmission line model, using parameters obtained from the ballistic conductance calculations made on both CNT conductors and junctions.

1.4 Outline of Thesis

The remainder of thesis is organized as follows:

Chapter 2 describes iodine doped conductor and junction calculations. Iodine has been found to be an effective conductance enhancer in doped CNT cables [3], [17]. Both CNT conductor and junction models are investigated. Note that iodine dopant per unit length was fixed while junction overlap was varied in order to investigate iodine doping effects.

Chapter 3 models double-walled tube conductors and junctions composed of CNT and copper. The copper-CNT nanomaterial has been shown (in published experiments) to offer greatly improved ampacity, as compared to pure CNT [4]. In the present work, several copper-CNT configurations are modeled, and chromium doping effects on junctions are also investigated.

Chapter 4 presents results on polyiodide doped CNT conductors and junctions. Compared to the atomic iodine dopants studied in chapter 2, this chapter considers 'molecular' iodine dopants (in all cases modeled at the electronic structure level). This chapter also addresses the issue of relaxation calculations, in particular convergence problems, and adopts an approximate modeling strategy to estimate the iodine distribution in 'molecularly' doped CNT cables. The effects of iodine doping on both metallic and semiconducting CNT are included in the computational investigation.

Chapter 5 formulates a transmission line model, used to estimate nanowire performance, applying conductor and junction analysis data presented in previous chapters. The transmission line is represented as series combination of CNT conductors and CNT junctions in order to estimate nanowire performance. Using copper conductor properties as a reference, the expected performance of various CNT and CNT-copper conductors is evaluated, on a specific conductivity basis.

Chapter 6 discusses the conclusion and contribution of this thesis.

Chapter 2: Iodine Doped CNT

2.1 INTRODUCTION

The development of conductors with high conductivity, high strength and low weight can benefit a wide range of electrical systems. Considerable previous research has focused on building high performance conductors. Among them the most promising materials for fundamentally improved conductors are carbon nanotube based composites. However, important challenges remain. While individual metallic single-walled CNT show outstanding potential, the performance of macroscopic CNT composites is much lower than expected. This may be due to both conductor and junction performance: (1) the difficulty of fabricating pure metallic CNT bundles means that the presence of semiconducting CNT will decrease the overall conductivity of the material [48]; and (2) electrons must inevitably pass through CNT junctions in any CNT network. The junctions are barriers for electron transport, which will further decrease the conductivity of the system. Experimental work [49] indicates that junction conductance for a metallic CNT junction is on the order of $0.1e^2/h$, which is $1/40$ the conductance of an individual metallic CNT. To address these issues, iodine doping has been found to be an effective means of conductivity enhancement. As reported in experimental references [3], the specific conductivity of a CNT cable shows as much as 300% improvement after iodine doping. As compared to a copper cable, the best CNT sample described in a recent experimental paper [3] shows improvement by a factor of three, in term of mass specific conductivity. Iodine doped CNT materials show great potential as high performance cables. Hence the present study investigated both doped conductors and doped junctions in order to understand iodine's function and its effects on CNT structures.

2.2 MODELING CONFIGURATION

This chapter considers only metallic CNT, specifically CNT(5, 5). Single CNT models are built to study conduction performance. Junction models formed by two partially overlapped CNTs are used to investigate electron transport between CNT's. To show the effects of iodine doping in different configurations, the doping mass ratio in single CNT models and the overlap length in doped junctions are chosen as model parameters. The analysis considered six CNT configurations:

- Single CNT, doped and undoped
- Junctions of two CNT's, aligned and misaligned, doped and undoped

The term 'aligned' refers to the positions of neighboring atoms in distinct nanotubes, and will be defined in a later section of the thesis. All calculations were performed for metallic (5, 5) single-walled carbon nanotubes.

All calculations were performed using the generalized gradient approximation (GGA) for the exchange-correlation functional parameterized by Perdew-Burke-Ernzerhof [50]. A single-zeta basis set is employed for both the carbon and iodine atoms. In this chapter, the cutoff radii for the basis orbitals are determined by setting the energy shift to 0.05 Ry [51]. The integration k-points in the Brillouin zone are chosen using a Monkhorst-Pack mesh [52]. For the relaxation calculations, the k-grid discretization is $1 \times 1 \times 4$ [43]. For conductance calculations, the k-grid discretization is set to $7 \times 5 \times 9$. The fineness of the real space mesh is controlled by setting the energy cutoff to 200 Ry [53]–[55]. The system is relaxed to an equilibrium state in which the maximum atomic force is less than 0.04 eV/Å [56], [57].

2.3 Results and Discussion

2.3.1 Iodine Doped CNT Conductors

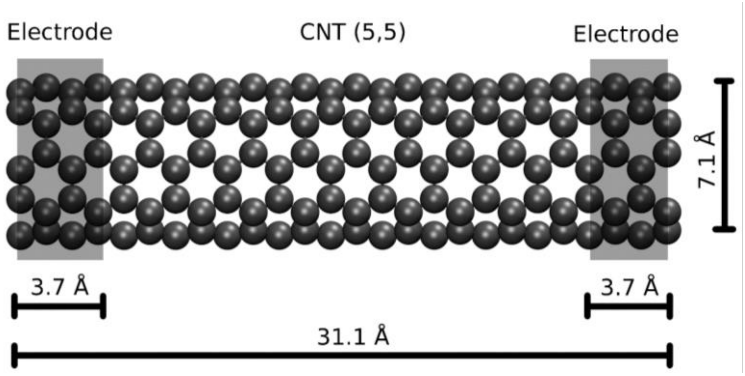

Figure 2.1: CNT(5, 5) calculation model

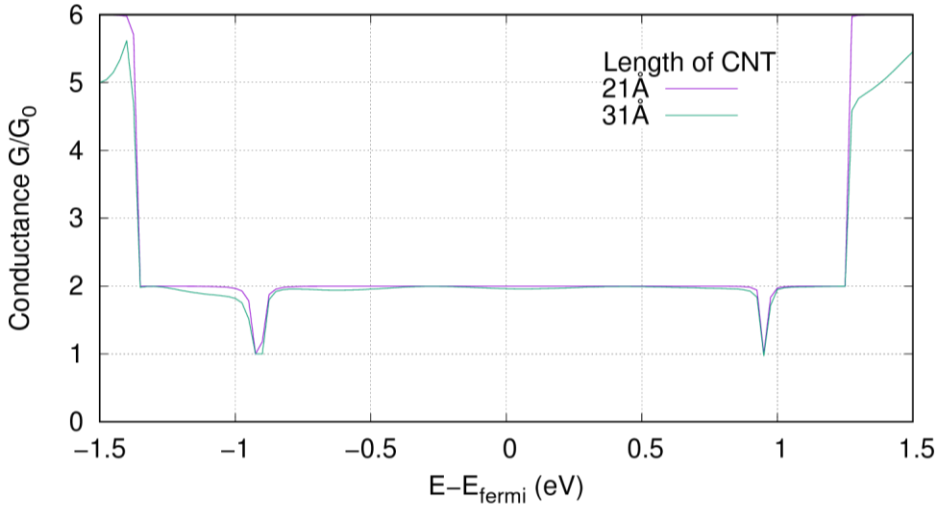

Figure 2.2: Conductance results for CNT(5, 5)

The conductance was first calculated for isolated nanotubes (Figure 2.1), at two different lengths. In this case the conduction calculations were performed after relaxation of the system to an equilibrium state. Consistent with published experimental data, Metallic CNT are ballistic conductors [58] and the nanotube conductance takes on the value $G = 2G_0$ $(\mathrm{T} = 2)$ at the Fermi Energy [25]. The analysis results are shown in Figure 2.2.

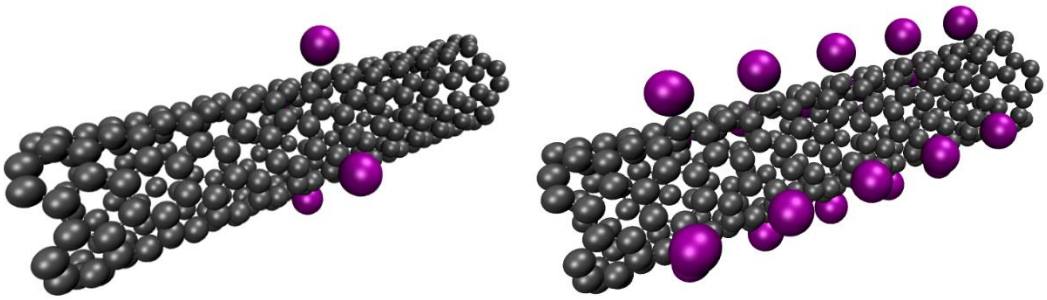

Figure 2.3: Iodine doped CNT models

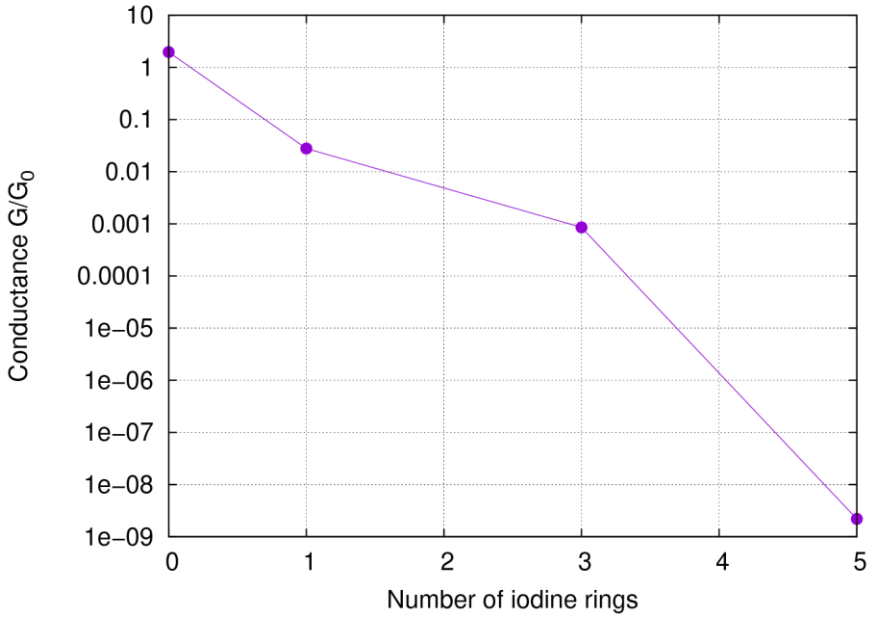

Figure 2.4: CNT conductance versus applied dopant

Next the conductance was computed for isolated nanotubes with various numbers of iodine atoms adsorbed to the CNT sidewall (Figure 2.3). Conduction calculations were performed after relaxation of the system to an equilibrium state. After geometry optimization, the axial separation distance of the iodine atoms was 5.1 Å, and the length of the carbon-iodine 'bond' was 2.2 Å. Note that published experimental research [59] has classified the iodine bonding as covalent, and that previous computational work [30]

modeling various covalently bonded addends (e.g. F) to CNT's indicates that such doping reduces CNT conductance.

Figure 2.4 shows the computed conductance, as a function of the number of iodine 'rings' bonded to the CNT sidewall. Consistent with previous research on covalent doping, iodine doping (in this case, in a ring configuration) sharply reduces CNT conductance.

2.3.2 Iodine Doped CNT Junctions

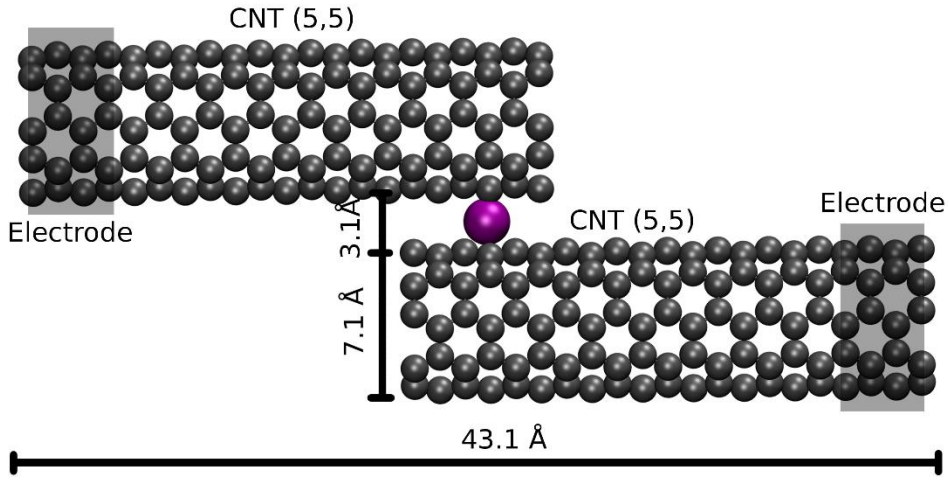

Figure 2.5: CNT junction model dimensions

Next the conductance was computed for both doped and undoped nanotube junctions, arranged as indicated in Figures 2.5 and 2.6. In this case, a geometric configuration was assumed and the conduction calculations were performed without relaxation of the system to an equilibrium state. The junction overlap was varied in increments of 9.9 Å, as shown in Figure 2.6, while the axial separation distance of the iodine atoms was fixed at 4.9 Å. Undoped configurations were obtained by simply removing the dopant atoms.

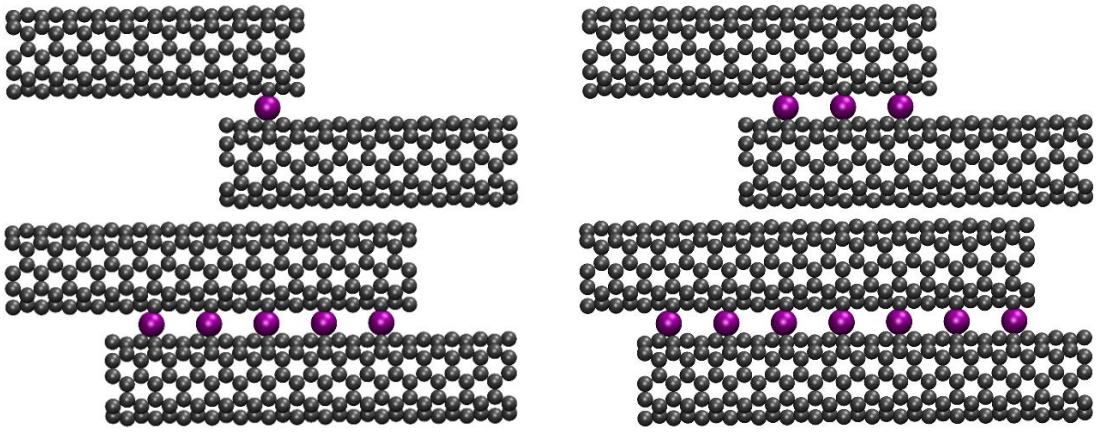

Figure 2.6: Junction model at different overlaps

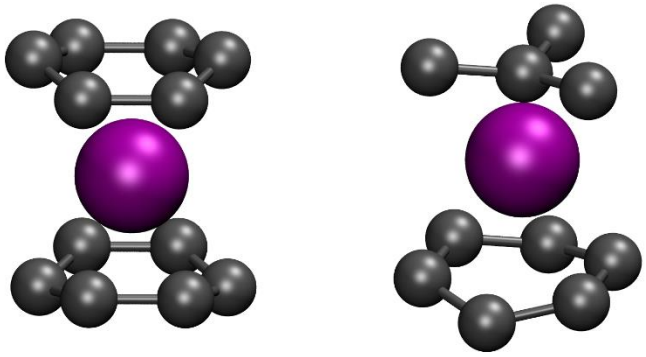

Figure 2.7: Aligned (left) and misaligned (right) configurations

Two different junction alignments were also analyzed. In the aligned case, the dopant atom and the adjacent carbon atoms formed a ‘sandwich’ substructure [43]. In the misaligned case, one nanotube was shifted axially. The two modeled configurations are depicted in Figure 2.7. Previous computational work has suggested that optimal doping treatments [43] and optimal overlap configurations [40] offer the possibility of constructing multi-junction networks which exhibit the excellent conductance properties of single nanotubes.

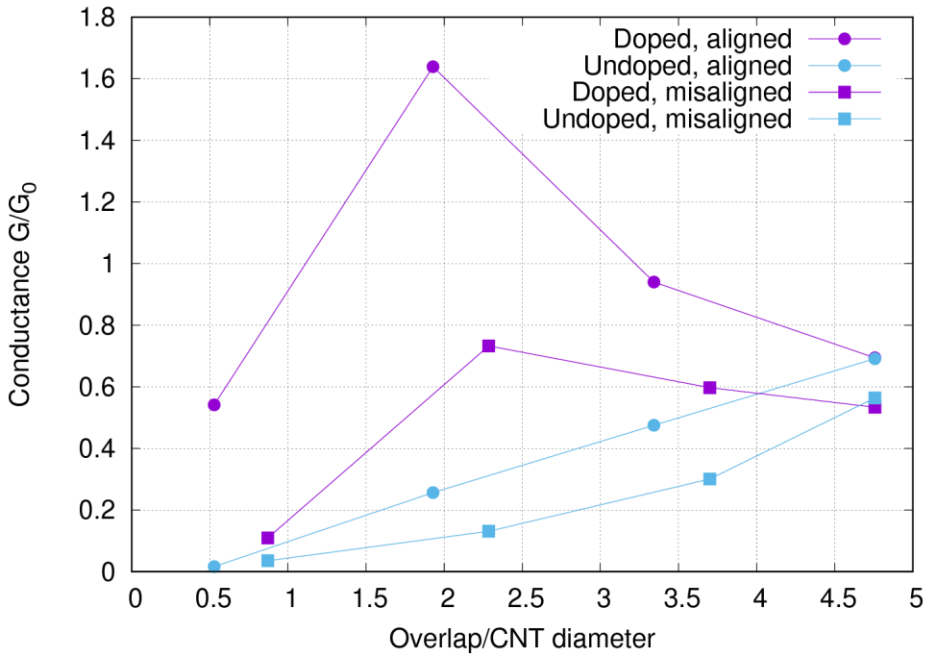

Figure 2.8: Junction conductance versus overlap

Figure 2.8 plots the results of the current calculations, indicating that a relative maximum in the conductance was observed only for the doped junction configurations (in the undoped cases, conductance increases monotonically with overlap). Note that the junction conductance is sensitive to alignment effects, in particular for doped junctions. At the best modeled combination of doping, alignment, and overlap, junction conductance is approximately eighty percent of that for a single ideal nanotube.

2.4 Conclusions

The following general conclusions are suggested: (1) the experimentally observed benefits of doping appear to be due to effects at the nanotube junctions, (2) the effects of doping on metallic nanotubes may be negative, and (3) for the metallic CNT junction model, the benefit of iodine doping depends on the junction structure. For the limited range

of overlaps investigated, an optimal overlap and alignment exist which achieve the best CNT junction performance.

The preceding results are consistent with observed conductivity improvements in CNT based conductors, after iodine doping, and may assist in the design and synthesis of stable CNT-based conductors for industrial applications. More research and analysis is clearly needed, including geometry optimization of junction models.

Chapter 3: Double Wall Carbon and Copper Tubes

3.1 Introduction

Copper has wide applications as a power and data transmission cable, due to its high conductivity and low cost. Although it has excellent electrical conductivity, considerable energy loss is nonetheless associated with the massive application of copper cabling. One possible way to improve the specific conductivity of copper based cabling is by adding carbon nanotubes, thus forming copper-CNT composite conductor [60], [61]. Since CNT is must lighter than copper, better mass specific electrical properties may be obtained. Experimental research [4] shows that copper-CNT nanomaterials may offer a 100 fold increase in ampacity, with little decrease in conductivity, as compared to copper. Other promising research [62], [63] suggest that the incorporation of CNT into copper can also improve the mechanical properties of the cable, so there is a great potential for copper-CNT as a material for next generation conductors.

This chapter is focused on modeling of copper-CNT nanomaterials, including both conductor and junction models. The effect of chromium as junction dopant is also considered. Chromium is shown (computationally) to be an effective dopant, for improving CNT junction conductance, and may provide stronger coupling between adjacent CNT, leading to improved junction performance [43].

3.2 Modeling Configuration

To investigate copper-CNT nanomaterial's conductance and junction behavior, this analysis considered thirty distinct copper, CNT, copper-CNT models. The study included both metallic (CNT(M)) and semiconducting (CNT(S)) nanotubes. The ten configurations are (each of these ten configurations included three models; a conductor model, an undoped junction model, and a doped junction model):

- Double wall copper tubes, two configurations (they differ in diameter)
- Double wall copper-CNT(M) and copper-CNT(S) tubes, four configurations
- Double wall CNT(M)-CNT(S) tubes, four configurations

The metallic CNT's are chirality (5, 5) (for the inner tubes) and (10, 10) (for the outer tubes). The semiconducting CNT's are chirality (9, 0) (for the inner tubes) and (18, 0) (for the outer tubes). The only modeled dopant was chromium.

Note that CNT's of chirality (9, 0) and (18, 0) may be referred to as metallic, since for metallic CNT the difference of vector index is an integer multiple of three: $n - m = 3t$ $(t = 0, 1, 2 \ldots)$[14]. However, previous work [15] and present calculations (Figure 3.1) indicate that these are borderline cases which actually incorporate a small band gap. Hence this work refers to CNT(9, 0) and CNT(18, 0) as semiconducting. Figure 3.1 depicts the band structures computed by SIESTA for CNT(9, 0) (on the left) and CNT(5, 5) (on the right) nanotubes. There is a small band gap predicted in the CNT(9, 0) case.

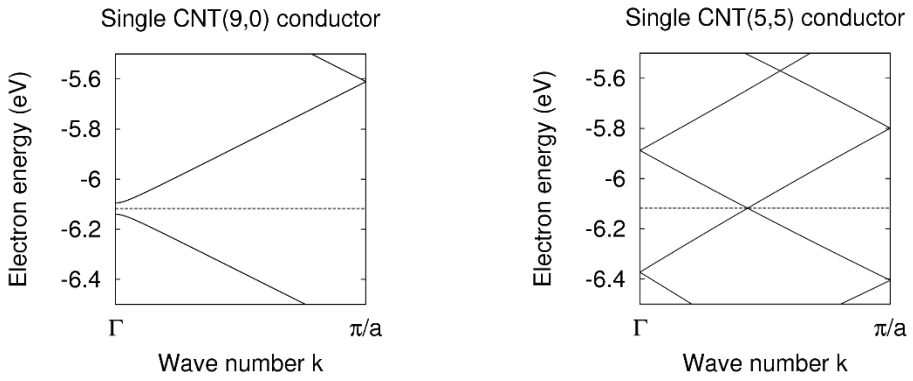

Figure 3.1: Band structure of CNT(9, 0) and CNT(5, 5)

In this chapter, all calculations are performed using a generalized gradient approximation (GGA) for the exchange-correlation functional, as parameterized by Perdew-Burke-Ernzerhof [50]. A single-zeta basis set is employed for both the carbon and copper atoms. The cutoff radii of the basis orbitals are determined by setting the energy

shift to the default value of 0.02 Ry [64]. The k-point is chosen using a Monkhorst-Pack mesh [52]. For the conductance calculation, the k-grid is $1 \times 1 \times 100$ [65]. The fineness of the real space mesh is controlled by setting the energy cutoff to 200 Ry [53]–[55].

3.2.1 Modeling Constraints

The following modeling constraints were applied, in order to limit computational cost and to satisfy certain periodicity constraints imposed by the SIESTA conductance modeling framework.

- Model size: models were composed of less than 1,000 atoms, except for the incommensurate DWCNT cases where the use of larger models was unavoidable.
- Relaxation: the models were not relaxed, due to convergence problems with the complex junction structure. So the locations of the dopant atoms in the junction model are assumed to match data from previous relaxed work [43].
- Junction overlap: junction overlap was limited to less than 3 Å.
- Copper tube model: a special lattice model was constructed for the copper tube. Its structure mimics a CNT, with the addition of interstitial atoms, approximating the (111) face of a copper crystal.
- Electrode model: atomic separation distances were reduced (by less than four percent) in some of the modeled tubes, in order to match unit cell lengths in the inner and outer tubes.

3.2.2 Double Wall Tube with Metallic CNT and Copper

In order to build double wall tube models composed of metallic CNT and copper, two methods are described in previous papers: (1) embedding CNT into bulk Cu, thus forming a copper-CNT matrix, as done by Ghorbani-Asl et al. [66], and (2) positioning the copper tube within a CNT, as done by Du et al [36]. The first method avoids the problem

of matching copper unit cells with CNT unit cells, however it requires many copper atoms. This is undesirable in electronic structure calculations, where 1000 atoms is the model limit in most cases. The second method reduces the atom count, however the lattice structure of the copper is not represented. In the present work, a special lattice of copper is constructed in order to overcome the drawbacks of previous methods.

As performed by SIESTA, the conductance calculation requires that both electrodes of the double wall model contain an integer number of unit cells. Since the length of the unit cell (for CNT(5, 5) 2.46 Å) and the atomic separation distance on the (111) face of copper (2.56 Å) are similar, we construct a copper tube model by mimicking the CNT geometry (interstitial atoms are added which correspond the face centered atoms in copper). A similar model is constructed in order to analyze the copper-CNT(S) system.

We use chirality (5, 5) and (10, 10) CNT's to model the copper-CNT(M) conductors. The unit cell length in the axial direction is 2.46 Å. The total model length is 29.5 Å (12 unit cells), and includes one electrode on each end, each of length 7.38 Å (3 unit cells). The model configuration is shown in Figures 3.2 and 3.3.

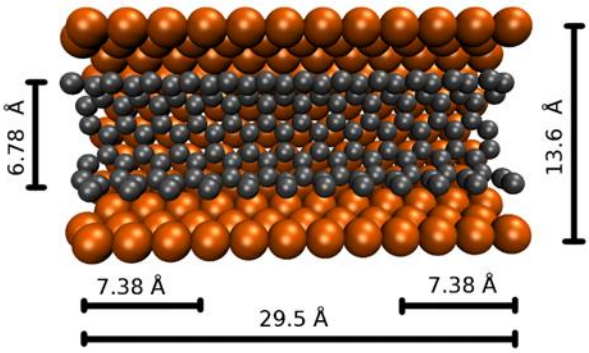

Figure 3.2: Dimension of the CNT(M)@Cu model

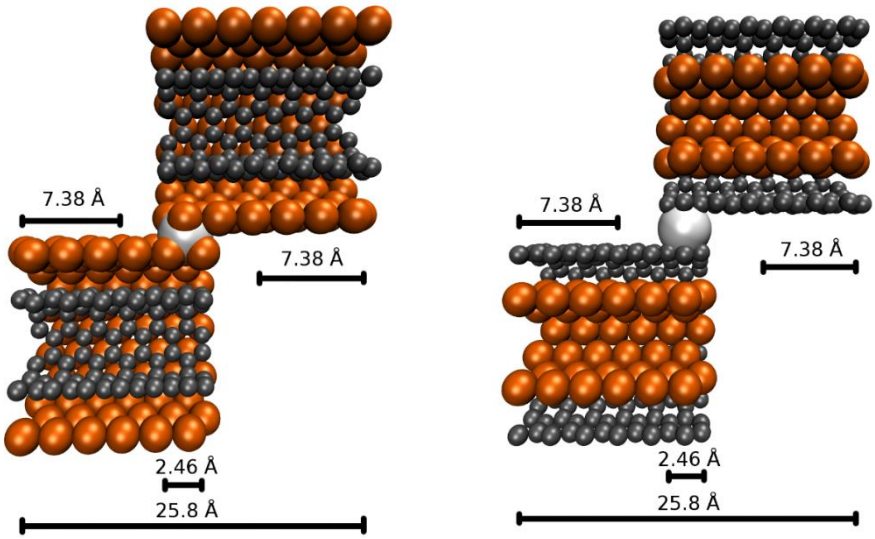

Figure 3.3: Dimensions of the CNT(M)@Cu (left) and Cu@CNT(M) (right) doped junctions

3.2.3 Double Wall Tube with Semiconducting CNT and Copper

We use chirality (9, 0) and (18, 0) CNT's to model the copper-CNT(S) conductors. The unit cell length in the axial direction is 4.26 Å. The total model length is 34.1 Å (8 unit cells), and includes two electrodes, each of length 8.53 Å (2 unit cells). The configuration is shown in Figures 3.4 and 3.5.

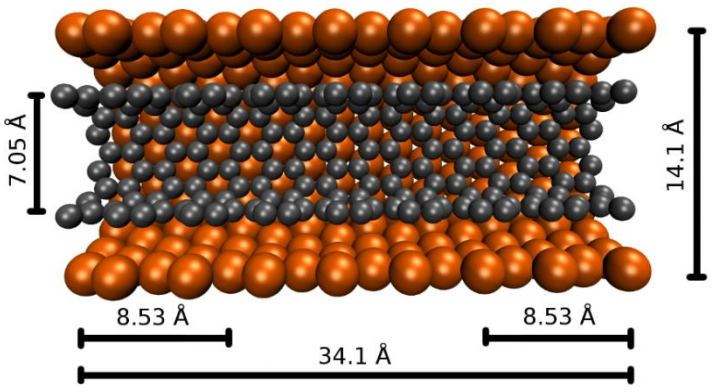

Figure 3.4: Dimensions of the CNT(S)@Cu model

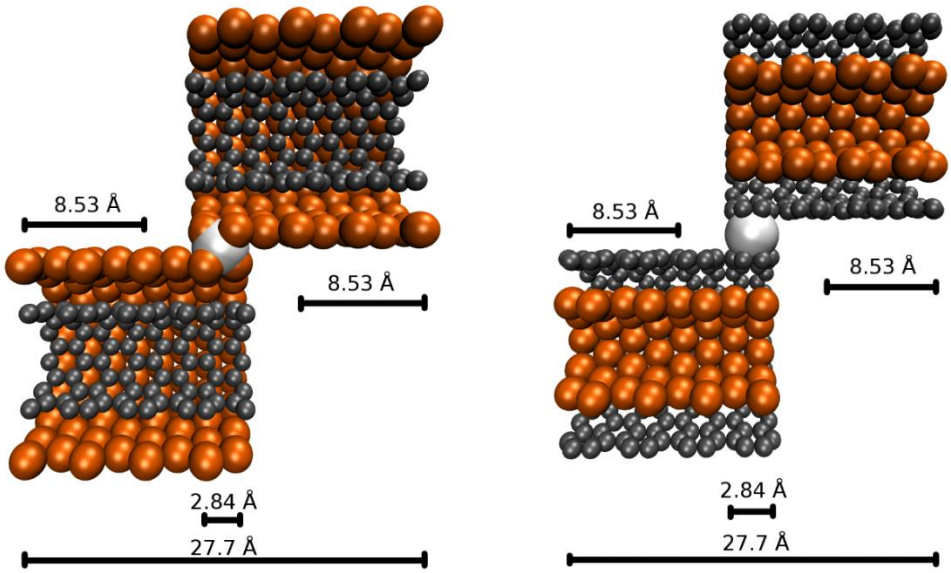

Figure 3.5: Dimension of the CNT(S)@Cu (left) and Cu@CNT(S) (right) doped junctions

3.2.4 Double Wall CNT

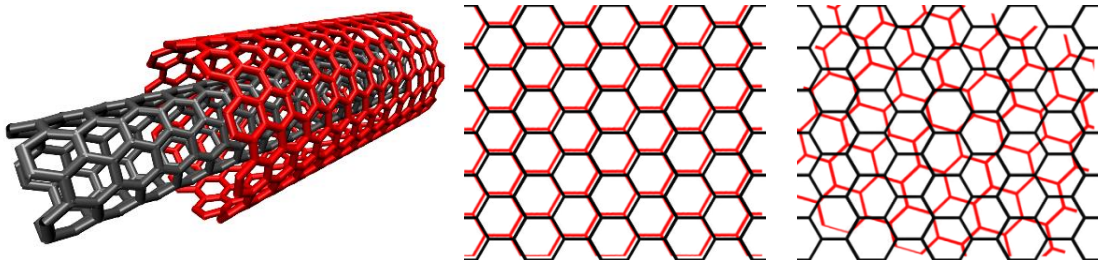

Figure 3.6: Double wall CNT (left) with CNT(5, 5)@CNT(10, 10) (naming convention is inner@outer), commensurate arrangement (center) and incommensurate arrangement (right) (Adapted from reference [67])

Modeling the CNT(M)@CNT(M) and CNT(S)@CNT(S) systems is simplified by the fact that the axial direction unit cell lengths for the inner and outer tubes are the same. The nanotubes are commensurate, as defined in Figure 3.6 (center).

Modeling the metallic and semiconducting double wall CNT systems is more complicated, since they are incommensurate CNTs. As stated by Liu et al [68],

> "Electronic structure calculations of incommensurate DWCNT's ... are challenging because a finite unit cell does not exist."

Here we model the incommensurate CNT(5,5)@CNT(18,0) and CNT(9,0)@CNT(10,10) systems by: (1) aligning 5 metallic unit cells with 3 semiconducting unit cells, then (2) uniformly compressing the semiconducting CNT by 3.76 percent. Table 3.1 shows the dimensions of the unit cells and the supercells employed to model the incommensurate DWCNT.

CNT chirality	Diameter (Å)	Unit cell length (Å)	Supercell length (Å)
(5, 5)	6.8	2.46	2.46×5=12.30
(10, 10)	13.6	2.46	2.46×5=12.30
(9, 0)	7.1	4.26	4.26×3=12.78 comp. to 12.30
(18, 0)	14.1	4.26	4.26×3=12.78 comp. to 12.30

Table 3.1: Dimensions of the cells used to model the DWCNT

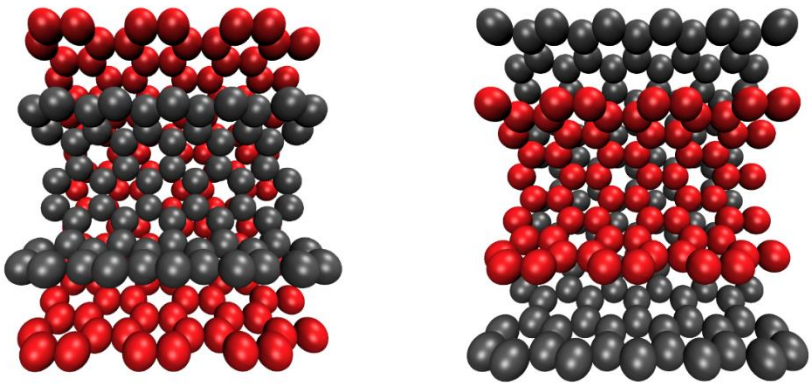

Figure 3.7: CNT(5,5)@CNT(18,0) (left) and CNT(9,0)@CNT(10,10) (right)

Figure 3.7 shows one supercell for the CNT(5,5)@CNT(18,0) and CNT(9,0)@CNT(10,10) systems. The red color denotes semiconducting CNT's, which are under homogeneous compression, at a magnitude of 3.76 percent. The total model (including electrode) length is 49.2 Å, which is four supercells. The electrode has one supercell on each side.

3.2.5 Junction Alignment

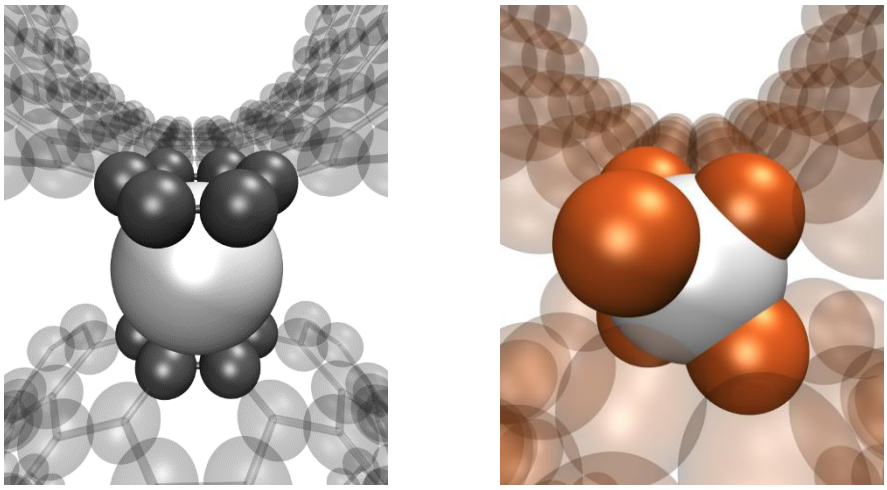

Figure 3.8: CNT-CNT junction (left) and copper-copper junction (right)

In the undoped CNT-CNT junctions (outer tube is CNT), the intertube separation distance is set to 3.3 Å, which is the interlayer spacing in graphite [69].

In the undoped copper-copper junctions (outer tube is copper), the intertube separation distance is set to 2.1 Å, so that the atomic separation distance for nearest neighbor atoms of the two tubes matches the separation distance for near neighbor atoms of the same tube (2.46 Å).

In the chromium doped CNT-CNT junctions, as shown in Figure 3.8 (left), the intertube separation distance is set to 3.6 Å, which yields an average separation distance

between the chromium atom and it's near neighbor carbon atoms of 2.34 Å (consistent with relaxed geometry calculations performed by Li et al. [43]).

In the chromium doped copper-copper junctions, as shown in Figure 3.8 (right), the intertube separation distance is set to 2.4 Å, so that the incremental increase in the intertube separation distance associated with the introduction of a dopant is the same in copper-copper case and the CNT-CNT case.

3.3 Results and Discussion

3.3.1 Scaled Conductance and Scaled Specific Conductance

The preceding models are used to compute scaled conductance and scaled specific conductance for the double wall tubes and the junctions. These variables are defined by:

$$Scaled\ conductance = \frac{G}{G_0}$$

$$Scaled\ specific\ conductance\ (tube) = \frac{G}{G_0}\frac{1}{\hat{m}_c}$$

$$Scaled\ specific\ conductance\ (junction) = \frac{G}{G_0}\frac{L_j}{m_j}, \quad m_j = 2\hat{m}_c L_j + m_d$$

where $\hat{m}_c$ is the mass per unit length of the conductor, L_j is the junction length (tube overlap), m_j is the mass associated with the junction, and m_d is the mass of the dopant (chromium). As discussed in the later chapter on nanowire modeling, it is the double wall tube specific conductance and the junction conductance which are of most interest in estimating nanowire performance. Hence the summary bar charts included in section 3.4, which compare the results for the various material systems, plot only the latter two variables.

3.3.2 Double Wall Tube with Copper and CNT

Figure 3.9-3.11 show the double wall configurations that were analyzed.

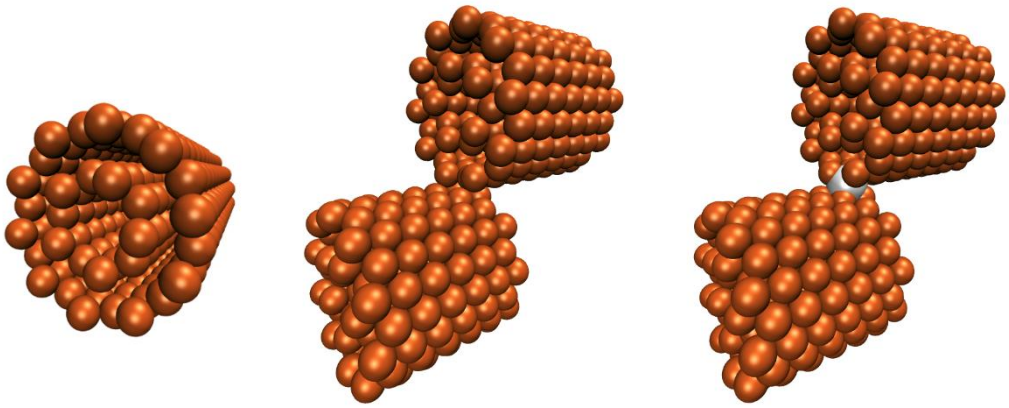

Figure 3.9: Conductor, undoped junction and doped junction for the Cu@Cu models

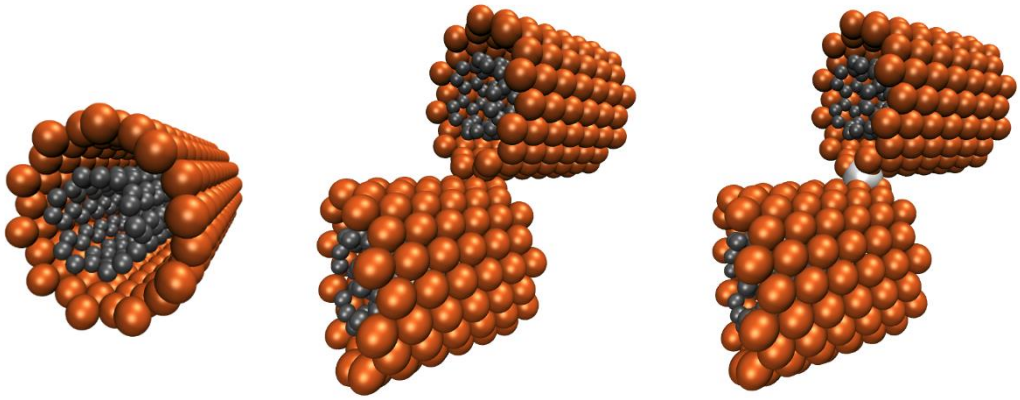

Figure 3.10: Conductor, undoped junction, and doped junction for the CNT(M)@Cu models

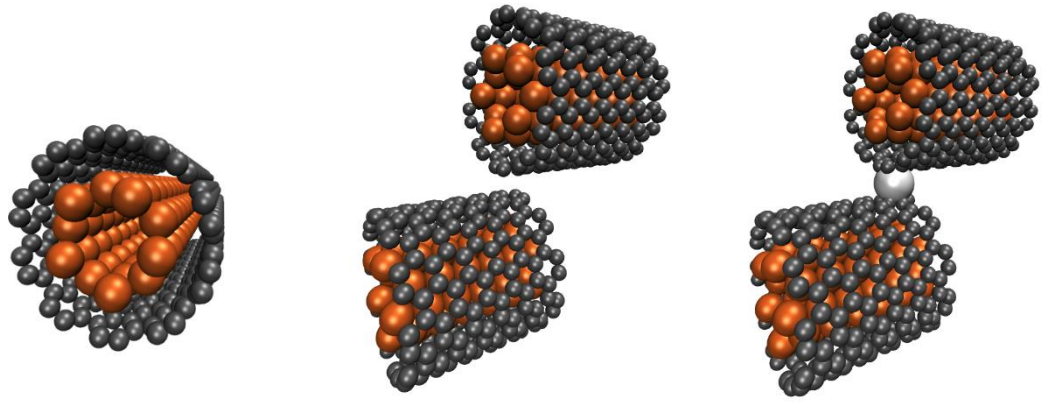

Figure 3.11: Conductor, undoped junction, and doped junction for the Cu@CNT(M) models

Figure 3.12 shows the analysis results for the copper and metallic CNT models, indicating that the presence of a junction is a huge disadvantage, in a conduction sense. Also, the beneficial effect of the chromium doping is very limited. Note that the mass specific conductance for all three conductors is similar.

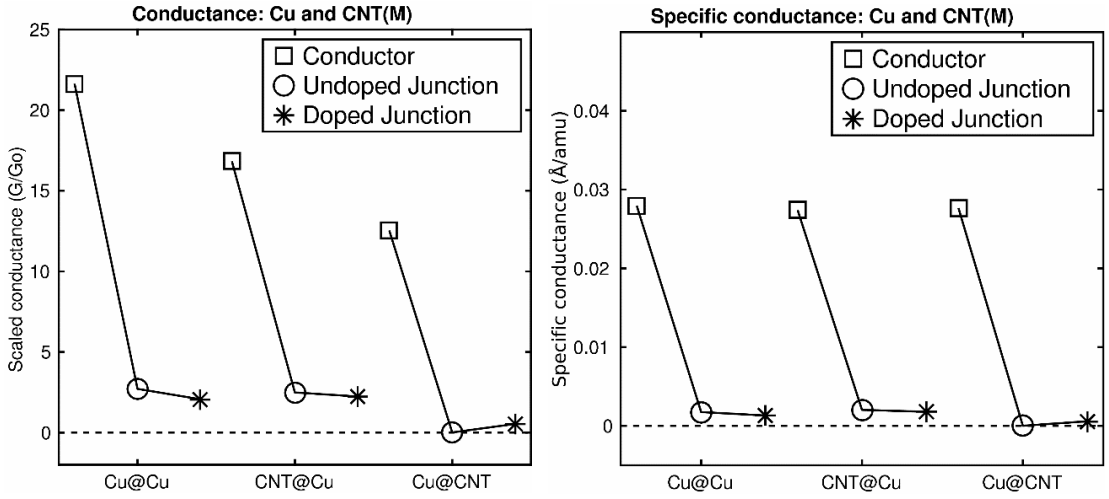

Figure 3.12: Conductance and specific conductance: copper and metallic CNT models

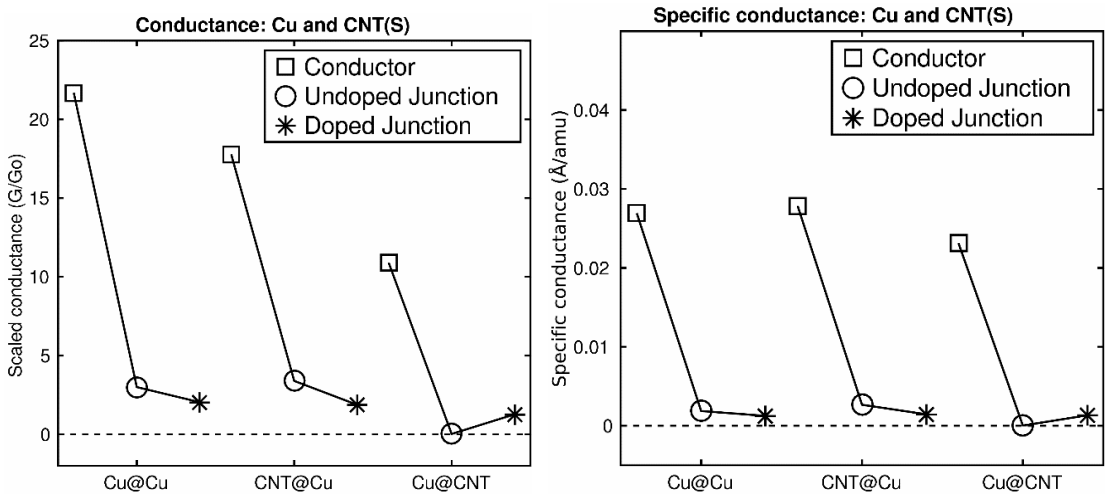

Figure 3.13: Conductance and specific conductance: copper and semiconducting CNT models

Figure 3.13 shows the analysis results for the copper and semiconducting CNT models. Note that for the undoped junction models, junctions formed by two outer copper tubes always outperform junctions formed by two outer CNT's, no matter what the type of CNT. Also note that introducing dopant at a copper-copper junction will have a negative effect on conductance, while introducing dopant at a CNT-CNT junction will have a positive effect. This result is consistent with published computational results indicating that chromium doping of CNT-CNT junctions will increase the 'coupling' between the CNTs [43].

3.3.3 Double Wall CNT

Figure 3.14 shows the modeled configurations for double wall CNT's.

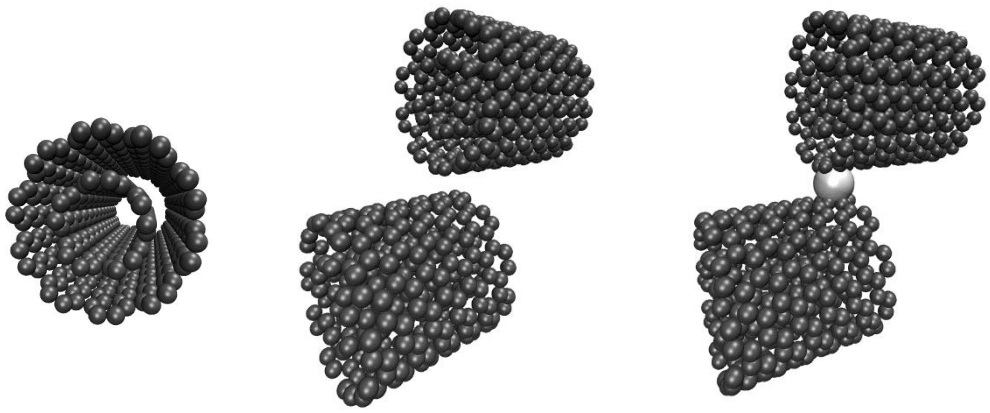

Figure 3.14: Conductor, undoped junction and doped junction for CNT(M)@CNT(M)

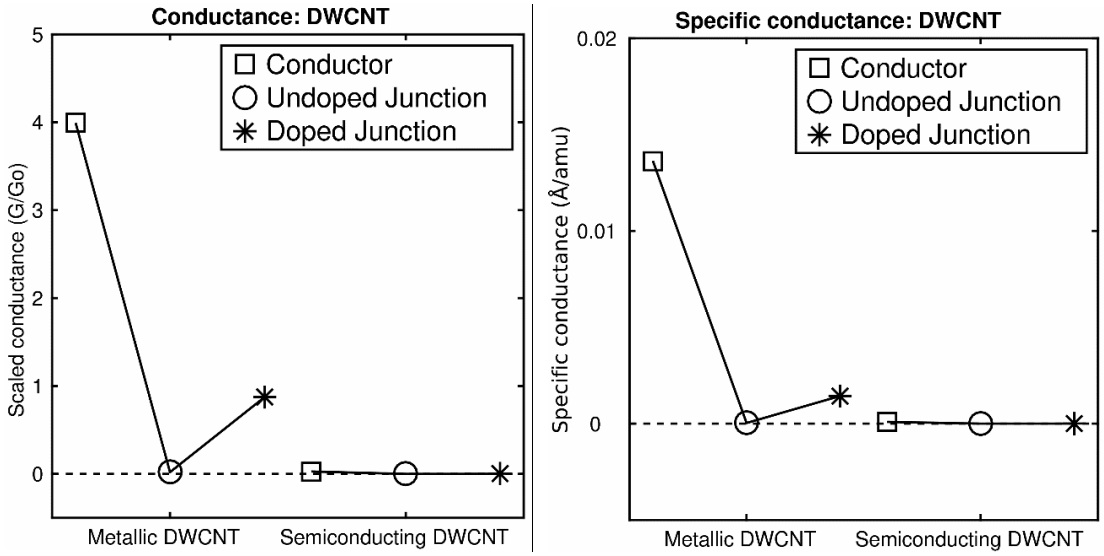

Figure 3.15: Conductance and specific conductance: commensurate CNT models (both CNT's metallic or both semiconducting)

In Figure 3.15, the results for the analysis of commensurate CNT's are presented. The conductance of a metallic DWCNT conductor is computed to be $4G_0$, consistent with published results [38]. The computed conductance for the undoped junction is consistent with previous calculations (see Figure 3.13) that the presence of CNT-CNT junctions is a huge disadvantage.

Notice that chromium doping has no effect on the performance of semiconducting junctions, while the other CNT-CNT junction models show improvement after chromium doping. This is due in part to the fact that the semiconducting electrodes have very limited conductance. As indicated in Figure 3.15, the conductance of the semiconducting DWCNT is almost zero; so when it is used as an electrode in a junction model, the junction conductance result is constrained by the electrode performance. By contrast, when the electrode has high conductance (e.g. Cu@CNT(S) in Figure 3.13), chromium's effect on the CNT-CNT junction performance is positive.

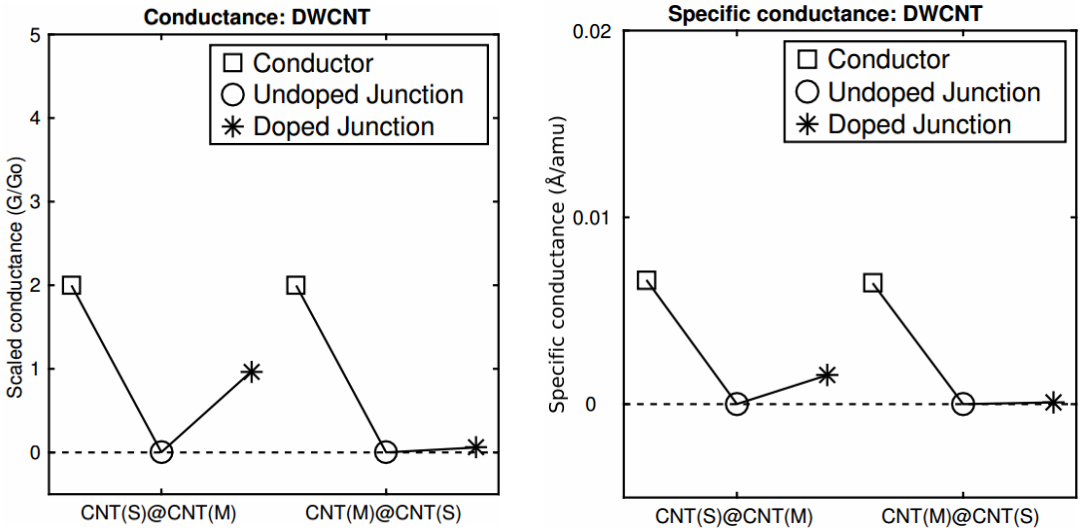

Figure 3.16: Conductance and specific conductance: incommensurate CNT Models (one metallic CNT, one semiconducting CNT)

The analysis results for the incommensurate DWCNT models are shown in Figure 3.16. Since only one of the two tubes is metallic, the DWCNT conductance is $2G_0$. Junctions composed of only CNT contacts are still a huge disadvantage. The beneficial effects of chromium are very limited for semiconducting CNT junctions.

3.4 CONCLUSIONS

Figure 3.17 compares the specific conductance of all of the double wall conductor models. Several conclusions are suggested: (1) double wall copper are the best conductors, and (2) replacing copper with CNT reduces conductance and offers (at best) no improvements in specific conductance.

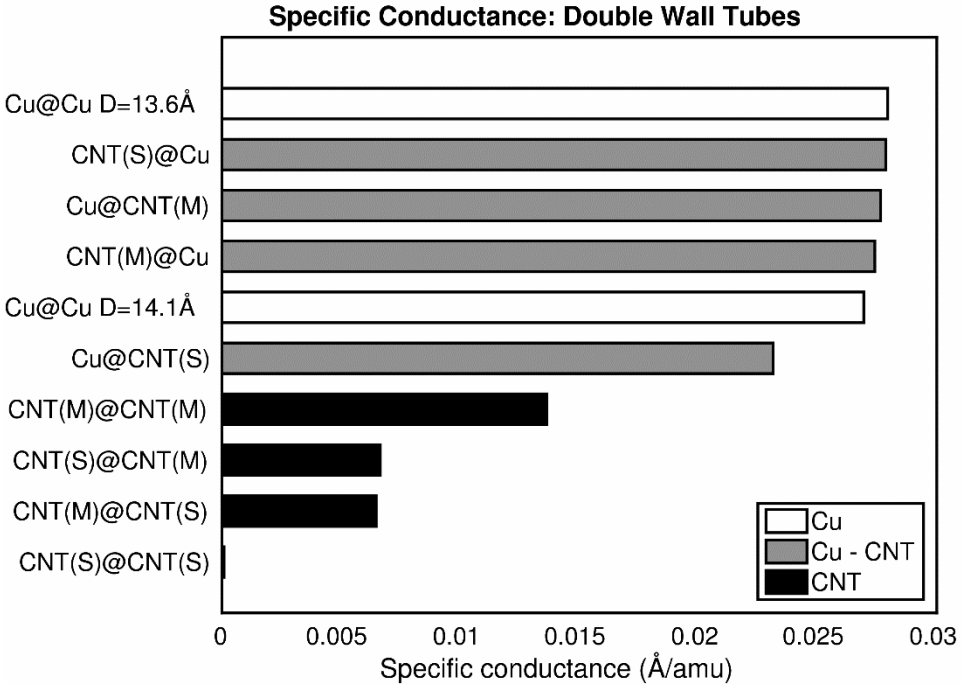

Figure 3.17: Specific conductance of the double wall models

Figure 3.18 compares the conductance of all of the doped junction models. It suggests two conclusions: (1) CNT(M)@Cu offers the best junction conductance, and (2) in general, junction conductance is higher when the outer tube is copper.

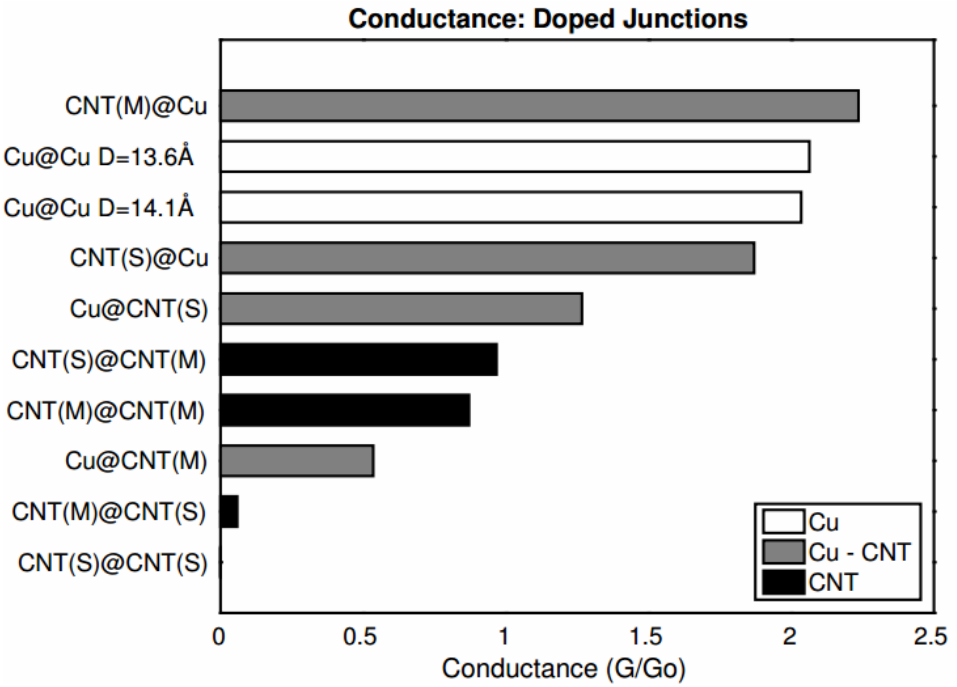

Figure 3.18: Conductance of the various junction models

Chapter 4: Polyiodide Doped CNT

4.1 Introduction

Iodine has been shown to be an effective dopant for CNT cables, increasing electrical conductivity [3], [17]. Published experimental data [3] indicates that the average specific conductivity of 18 weight percent iodine doped CNT cables is similar to that of copper; the best performance is approximately triple that of copper. In Chapter 2, which modeled the use of iodine atoms to dope CNT conductors and junctions, the interaction between iodine atoms was negligible. However, in general the performance of iodine doped systems may be affected by iodine atom interactions. An example is the presence of iodine in polyiodide form, as described in experimental papers [3], [70], which have suggested that I_3^- and I_5^- polyiodide chains may be formed during the doping process. An iodine chain structure located inside CNT's was also observed in experiments performed by Fan et al [71].

Based on TEM images of iodine doped CNT [3], the iodine distribution in doped CNT cables is speculated to consist of: (1) interstitial dopant atoms concentrated near CNT 'contacts' and (2) randomly distributed dopant atoms scattered across CNT surfaces. To better understand the effects of polyiodide doping, the analysis which follows considers CNT's doped with polyiodide structures (note that the present model is formulated at the electronic structure level, no molecular structure is imposed). Here the interaction of both metallic and semiconducting CNT's with polyiodides is investigated.

4.2 Modeling Configuration

The modeled CNT are metallic CNT(5, 5) and semiconducting CNT(8, 0), with diameters 7.1 Å and 6.4 Å respectively. Note that the smallest energetically stable CNT has diameter of 4 Å [72].

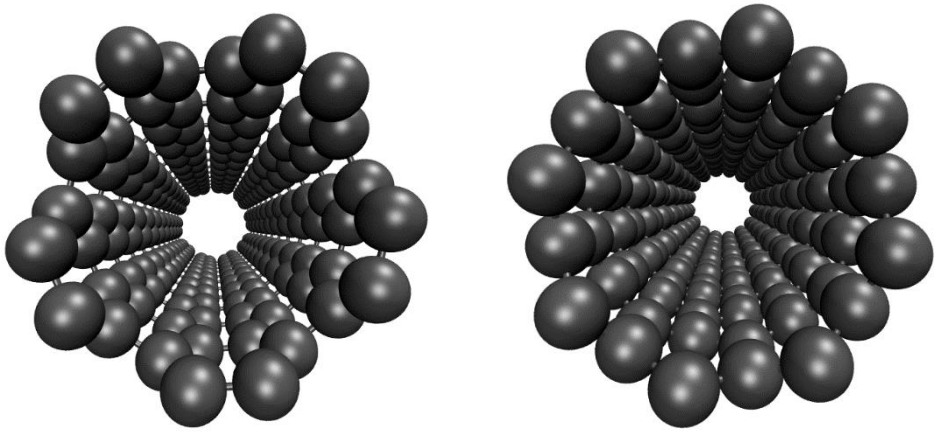

Figure 4.1: CNT(5, 5) (left) and CNT(8, 0) (right)

The following iodine doped system configurations were modeled, for both metallic and semiconducting CNT. In some configurations, dopant weighting was also varied.

- CNT conductors with aligned doping (relaxed)
- CNT conductors with random doping (relaxed)
- CNT conductors with interstitial doping (relaxed)
- CNT junctions with interstitial doping (unrelaxed)

In this chapter, an equilibrium calculation is first performed at the molecular level, using a Universal Force Field [73], and the results are then processed in a SIESTA calculation. All electronic structure calculations are performed using a generalized gradient approximation (GGA) for the exchange-correlation functional as parameterized by Perdew-Burke-Ernzerhof [50]. A single-zeta basis set is employed for both the carbon and the iodine atoms. The cutoff radii for the orbital basis functions are determined by setting the energy shift to 0.0036 Ry (50 meV) [38]. The k-point is chosen using a Monkhorst-Pack mesh [52]. For the relaxation calculations, the k-grid has dimensions $1 \times 1 \times 4$ [43]. For the conductance calculations, the k-grid dimensions are $1 \times 1 \times 9$ [38], [56]. The

fineness of the real space mesh is controlled by setting the energy cutoff to 200 Ry [53]–[55].

Two problems have been encountered in performing relaxation calculations using SIESTA: (1) In some configurations the equilibrium calculation will not converge, in particular this problem arises in complex doped junction configurations, and (2) in some cases the calculation will converge on high energy local equilibrium configurations. To address these problems, the following procedures have been applied:

The modeled system was relaxed using a two-step process. First, geometry optimization is performed at the molecular level using Avogadro [74], which employs a Universal Force Field [73]. Often this produces a starting configuration which will allow a SIESTA equilibrium calculation to converge to a low energy equilibrium.

In the second step, the Avogadro results are 'optimized' in SIESTA. The SIESTA relaxation computes the electronic structure; optimization will stop when the maximum atomic force falls below 0.04 eV/Å [56], [57]. In those cases where the SIESTA equilibrium calculation is still unable to converge (typically complex doped junction models), atom positions in the SIESTA conduction calculation are taken from simplified models whose symmetry properties allowed the SIESTA equilibrium calculations to converge.

4.3 Results and Discussion

Chapter 2 described the conductance properties of CNT's and CNT junctions doped with atomic iodine. This section describes the conductance properties of CNT's and CNT junctions with polyiodide doping. Section 4.3.1 presents the results for the doped conductors (both metallic and semiconducting). Section 4.3.2 presents the results for the doped junctions (both metallic and semiconducting).

4.3.1 Polyiodide Doped CNT Conductors

The polyiodide doped conductor models investigated single nanotube and dual nanotube configurations. In the single nanotube configurations, both 'aligned' and 'random' doping patterns were modeled. In the dual nanotube configuration, only 'interstitial' doping patterns were modeled. The doping geometries are illustrated in the figures which follow.

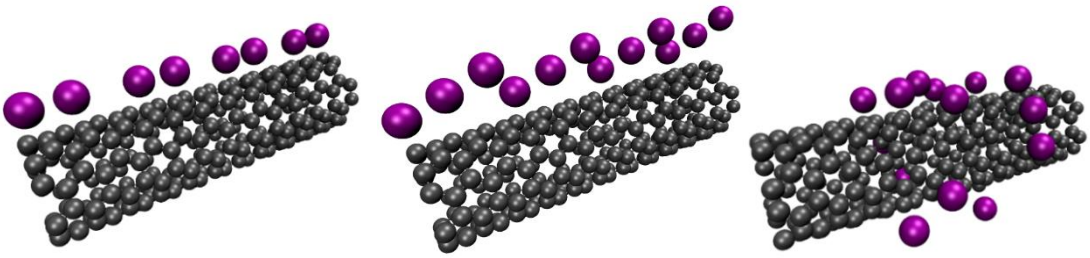

Figure 4.2: Metallic CNT(5, 5) model with aligned 0.7 iodine/unit cell (left), aligned 1.0 iodine/unit cell (center), random 2.3 iodine/unit cell (right)

Figure 4.2 shows the modeled single metallic nanotube configurations. The first and second models assume 'aligned' dopant atoms, with 0.7 iodine atoms per unit cell and 1.0 iodine atoms per unit cell respectively. The third model depicts the random doping pattern. In the case of the metallic CNT's, the electrodes were left undoped.

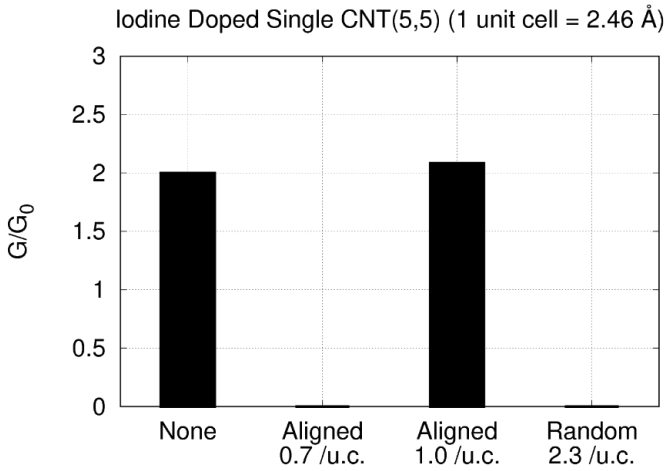

Figure 4.3: Conductance for the metallic CNT models

Figure 4.3 shows the computed conductance for the doped metallic CNT's (for comparison, the conductance for an undoped metallic CNT is shown with the label 'None'). The results indicate that the effect of doping a single metallic CNT is to reduce conductance, or at best to break even. Note the relatively heavy doping in the randomly doped configuration, which shows that the iodine distribution is important.

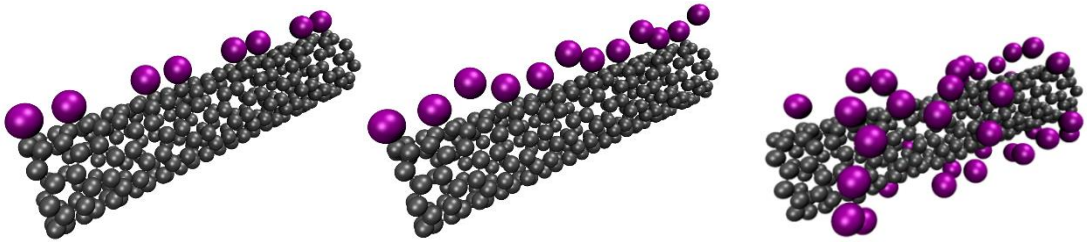

Figure 4.4: Semiconducting CNT(8, 0) model with aligned 1.0 iodine/unit cell (left), aligned 1.5 iodine/unit cell (middle), random 4.9 iodine/unit cell (right)

Figure 4.4 shows the modeled single semiconducting nanotube configurations. The first and second models assume 'aligned' dopant atoms, with 1.0 iodine atoms per unit cell and 1.5 iodine atoms per unit cell respectively. The third model depicts the random doping pattern. In the randomly doped model for the semiconducting CNT, the electrodes were doped.

Figure 4.5 shows the computed conductance for the doped semiconducting CNT's (for comparison, the conductance of an undoped semiconducting CNT is shown with the label 'None'). The effect of doping the semiconducting CNT was negligible. Note the relatively heavy doping in the randomly doped configuration, and that all the doped semiconducting CNT have poor conductance.

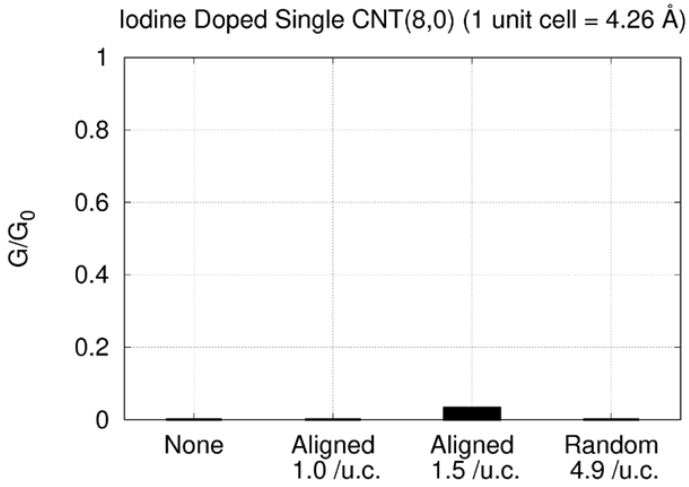

Figure 4.5: Conductance for the semiconducting CNT models

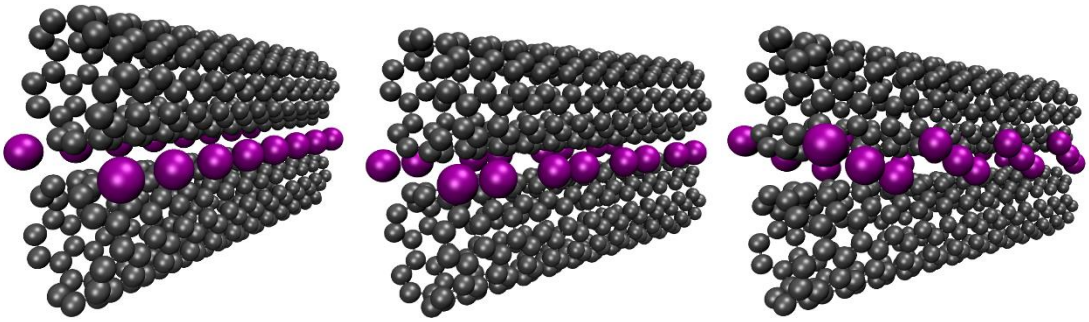

Figure 4.6: Interstitially doped metallic CNT(5, 5) with unrelaxed 1.3 iodine/unit cell (left), relaxed 1.3 iodine/unit cell (center), relaxed 2.0 iodine/unit cell (right)

Figure 4.6 shows the modeled dual metallic nanotube configurations. In the first model, the iodine atoms were uniformly spaced and the model was unrelaxed. The second and third models analyzed relaxed configurations, with 2.0 and 3.0 iodine atoms per unit cell respectively. The computed conductance results, provided in Figure 4.7, again indicate that iodine doping of the metallic tubes reduces conductance.

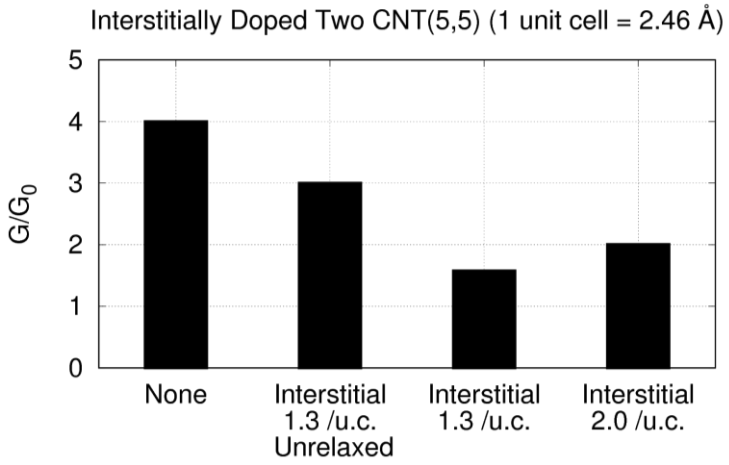

Figure 4.7: Conductance of interstitially doped two CNT(5, 5)

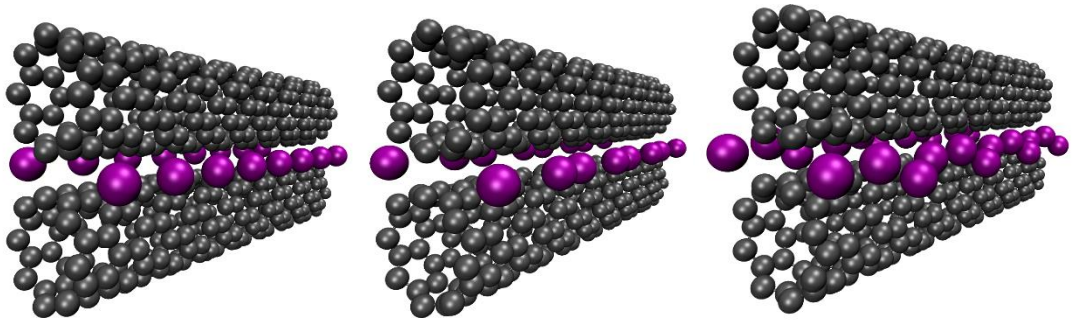

Figure 4.8: Interstitial doped semiconducting CNT(8, 0) with unrelaxed 2.0 iodine/unit cell (left), relaxed 2.0 iodine/unit cell (middle), relaxed 3.0 iodine/unit cell (right)

Figure 4.8 shows the modeled dual semiconducting nanotube configurations. In the first model, the iodine atoms were uniformly spaced and the model was unrelaxed. The second and third models analyzed relaxed configurations, with 2.0 and 3.0 iodine atoms per unit cell respectively. The computed conductance results, provided in Figure 4.9, indicate that polyiodide doping has the potential to greatly improve semiconducting CNT performance; however efficient distribution of the dopant is critical.

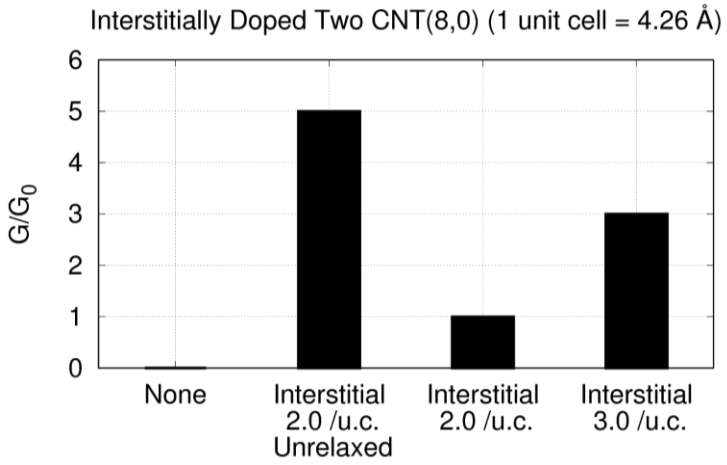

Figure 4.9: Conductance of interstitially doped dual CNT(8, 0)

4.3.2 Polyiodide Doped CNT Junctions

The polyiodide doped CNT junction models investigated dual nanotube configurations, at various overlaps, in interstitial doping configurations. The dopant per unit length was varied, and both metallic and semiconducting tubes were analyzed. In general, relaxation calculations for the doped CNT junctions failed to converge. Hence the junction models were constructed by removing carbon atoms from a relaxed model of the interstitially doped CNT's depicted in Figures 4.6 and 4.8.

Figure 4.10 depicts doped metallic nanotube junctions, at two different overlaps (junction overlap was varied from 2 to 10 unit cells in the metallic CNT junction models). Figure 4.11 shows the computed conductance results. Note that the result indicated by the red box in Figure 4.11 is used in the nanowire performance calculations discussed in Chapter 5. Overall the analysis suggests that polyiodide doping has the potential to greatly improve junction conductance.

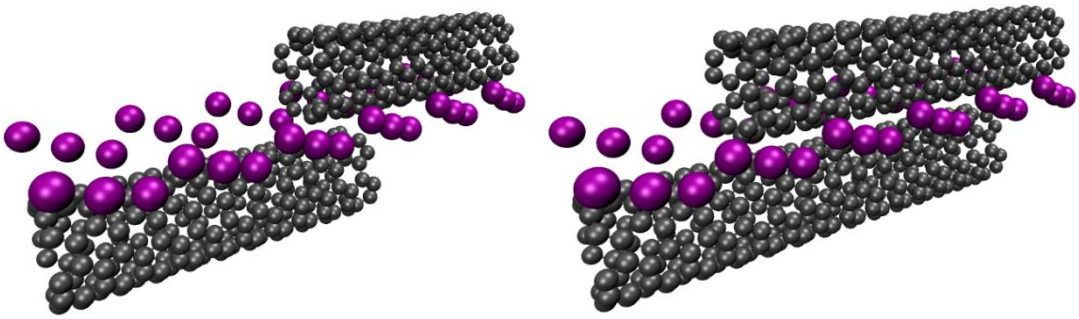

Figure 4.10: Doped metallic CNT(5, 5) junction with overlap equals to 2 unit cells (left) and 10 unit cells (right)

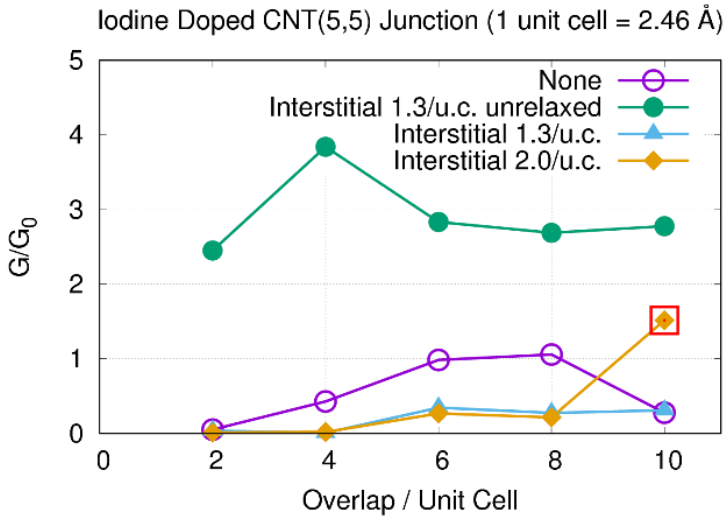

Figure 4.11: Conductance of metallic CNT(5, 5) junction

Figure 4.12 depicts doped semiconducting nanotube junctions, at two different overlaps (junction overlap was varied from 0.7 to 4.7 unit cells in the semiconducting CNT junction models; unit cell lengths differ between the metallic and semiconducting CNT's). Figure 4.13 shows the computed conductance results. Note that the result indicated by the red box in Figure 4.13 is used in the nanowire performance calculations discussed in Chapter 5. Again the overall analysis suggests that polyiodide doping has the potential to greatly improve junction conductance.

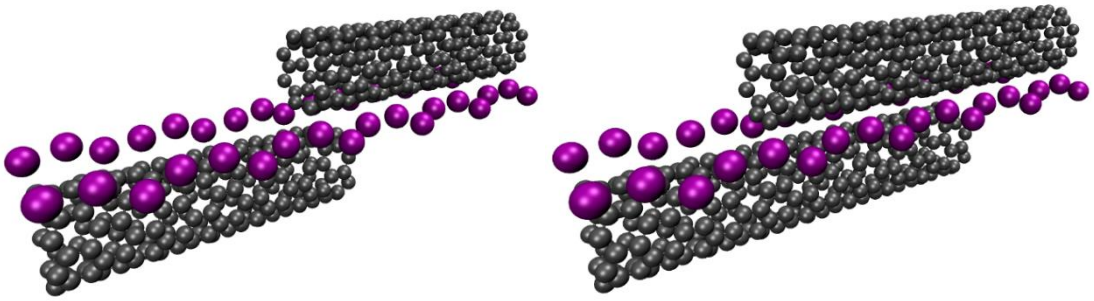

Figure 4.12: Doped CNT(8, 0) junction with overlap equals to 0.7 unit cells (left) and 4.7 unit cells (right)

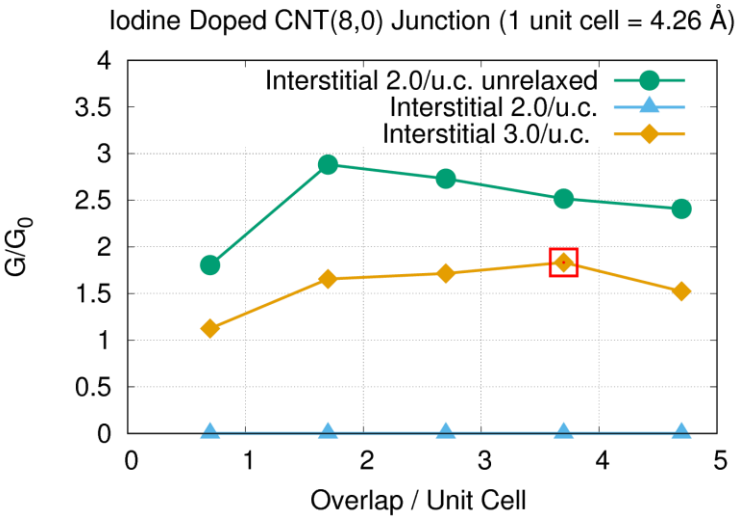

Figure 4.13: Conductance of semiconducting CNT(8, 0) junction

Note that the unrelaxed polyiodide model indicates high conductance. One possible explanation for the enhanced conductance is charge transfer in an ordered polyiodide structure, in which case the electrical conduction mechanism may be a Grotthuss mechanism [75], [76]. Published work indicates that the latter mechanism can transport charge, without mass transport, in polyiodide materials [77]. Current explanations of the effects of iodine doping on CNT conductance focus on iodine as p-type dopant for the CNT

[31], [78]. The mechanism proposed here suggests that iodine can also serve as a separate conductor, in ordered polyiodide form (Grotthuss mechanism). Note that published experimental observations on iodine doped CNT have identified a helix chain structure for polyiodide located inside the CNT [71]. Note that 'ordered' polyiodides obtained by: (1) location within a CNT [71], or (2) the confinement effects of multiple external CNT's [3] may lead to fundamental improvements in iodine doped CNT system conductance.

4.4 CONCLUSIONS

The results presented in this chapter suggest that polyiodide doping can greatly improve CNT system conductance. Fundamental improvements in the performance of doped semiconducting CNT conductors and junctions may be due to charge transfer within the polyiodide, for example via a Grotthuss mechanism. For CNT cables constructed of a mix of metallic and semiconducting tubes, the overall effect of iodine doping appears to be an improvement of as much as 300% in specific conductivity [3].

Chapter 5: Transmission Line Model

5.1 INTRODUCTION

In this chapter a nanowire is modeled as a transmission line consisting of a set of conductors, each with a length no greater than the mean free path for the conductor material, joined by discrete 'junction' resistors. The mass and conductivity properties of the transmission line components are taken from the ballistic conductance analysis described in previous chapters. The assumed model, shown in Figure 5.1, is inspired by experimental measurements on CNT networks [79]. Estimates of the mean free path for the conductor materials are taken from the literature [22], [23], [80].

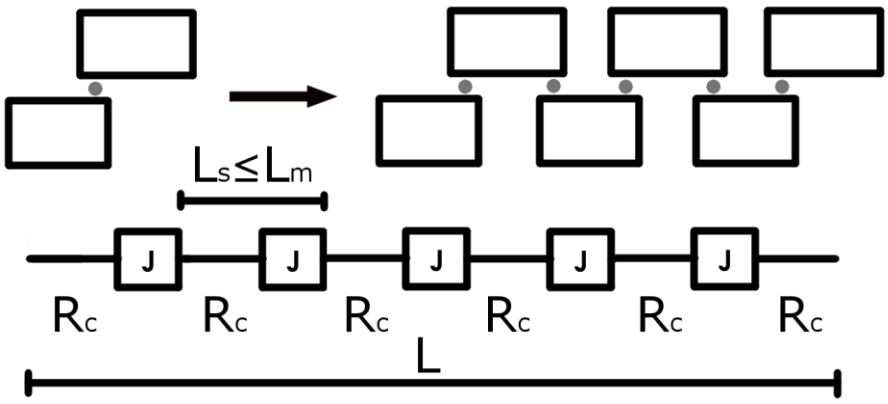

Figure 5.1: Transmission line model

The mass per unit length and resistance per unit length of the transmission line are determined by the conductor resistance R_c, junction resistance R_j, conductor mass per unit length $\hat{m}_c$, and added mass per junction m_j^{add}, all determined from the models described in previous chapters, and by the mean free path (L_m) of an electron in the conductor. Adopting the product of mass per unit length and resistance per unit length as performance metrics for a nanowire, define M using

$$\frac{1}{M} = \frac{\rho}{\sigma} = \frac{m}{L} \times \frac{R}{L} = (\hat{m}_c + \frac{m_j^{add}}{L_m}\hat{n})(\frac{R_c + R_j}{L_m})\hat{n}$$

where the number of junctions per unit free path is

$$\hat{n} = \frac{n}{L/L_m}$$

and n is the number of junctions in a transmission line of length L.

The plots which follow employ the metric M to estimate the performance of nanowires fabricated using the various material systems considered in previous chapters. Specifically, they plot the relative specific conductivity M/M_{ref} versus the number of junctions per unit mean free path $(\hat{n})$ for each material system, where M_{ref} is a reference value for the chosen metric. The reference value is the ratio of electrical conductivity to mass density for pure copper, readily available in the literature. Note that for the minimum value of $\hat{n} = 1$ indicated in the plots, the number of junctions is just sufficient to permit ballistic conductance. Additional junctions add parasitic mass and resistance, reducing nanowire performance. The plots assume a mean free path of 50 nm for copper [80], and 100 nm to 1,000 nm for the CNT's [22], [23].

5.2 CONSISTENCY CHECK

The specific conductivity metric (M) has the functional form

$$M = M(R_c, R_j, \hat{m}_c, m_j^{add}, L_m, \hat{n})$$

Assuming an ideal nanowire configuration in which $R_j = 0, m_j^{add} = 0, \hat{n} = 1$, for the two copper-copper tube models (D = 13.6Å and D = 14.1Å) analyzed in chapter 3, and a mean free path of $L_m = 50\ nm$ for the copper, the transmission model line indicates

$$M = M(R_c, 0, \hat{m}_c, 0, 50nm, 1) = 0.98\ M_{ref} \quad D = 13.6\text{Å}$$

$$M = M(R_c, 0, \hat{m}_c, 0, 50nm, 1) = 0.95\ M_{ref} \quad D = 14.1\text{Å}$$

These agree well with the expected results ($M = M_{ref}$). This check suggests that the conductance values computed by SIESTA are consistent with published data on the room temperature mean free path of copper.

5.3 Results and Discussion

5.3.1 Double Wall Tube with Copper and CNT

All combinations of copper-CNT conductors and junctions, and the best configurations of DWCNT based conductors and junctions, were selected for nanowire analysis in this chapter and are shown in Table 5.1.

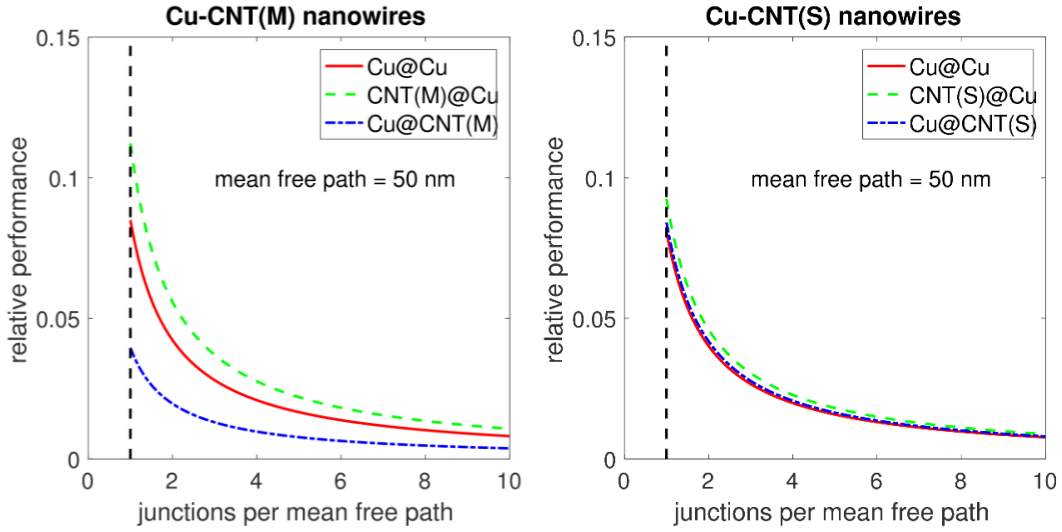

Figure 5.2: Performance evaluation for the copper-CNT nanowires

For the Cu-CNT nanowires, as shown in Figure 5.2, the best performance is obtained using a metallic CNT inside a copper tube. In this case the junctions will be formed by two adjacent copper tubes. Even in the best case, the estimated performance is less than 15 percent of that for conventional copper wires. Note that 'excess' junctions

significantly degrade performance, and the same effect is observed in all of the nanowire models.

	$\frac{1}{R_c}(\frac{G}{G_0})$	$\frac{1}{R_j}(\frac{G}{G_0})$	$\hat{m}_c\ (\frac{amu}{\text{Å}})$	$m_j^{add}\ (amu)$
Cu@Cu D=13.6A	21.64	2.06	774.6	1988.5
CNT(M)@Cu	16.82	2.24	614.0	1587.0
Cu@CNT(M)	12.54	0.54	453.4	1185.5
Cu@Cu D=14.1A	21.68	2.03	804.9	2064.2
CNT(S)@Cu	17.78	1.87	638.1	1647.2
Cu@CNT(S)	10.90	1.27	471.2	1230.0
CNT(M)@CNT(M)	3.99	0.87	292.8	784.0
CNT(S)@CNT(S)	0.03	0.00	304.3	812.7
CNT(S)@CNT(M)	1.99	0.97	300.6	803.5
CNT(M)@CNT(S)	1.99	0.12	308.4	823.0

Table 5.1: Computational predictions of copper-CNT model in transmission line model

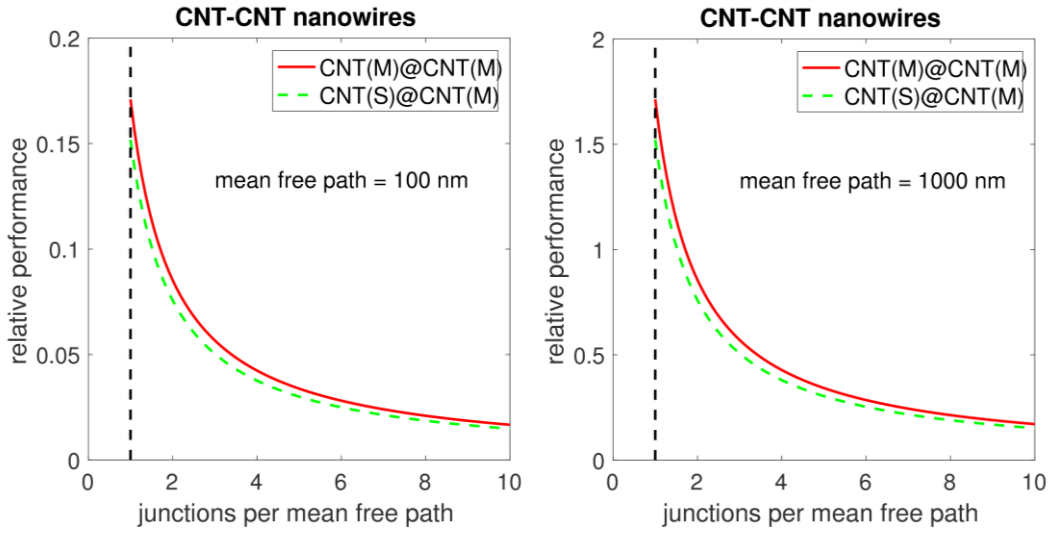

Figure 5.3: Performance evaluation on CNT-CNT nanowires

In the selected high performance cases shown in Figure 5.3, the nanowire junctions are formed by two metallic CNT's. The CNT-CNT configurations with an outer semiconducting CNT incorporate junctions are nearly open-circuit. For the CNT-CNT nanowires, the best performance is obtained using double wall metallic CNT's. The estimated nanowire performance depends strongly on the assumed mean free path. For a mean free path of one micrometer, the best estimated performance exceeds that of conventional copper wires by more than seventy percent (at the minimum junction count).

5.3.2 Polyiodide doped CNT

The high performance combinations of iodine doped CNT conductors and junctions, selected for nanowire analysis in this chapter, are shown in Table 5.2. The selected junction data is highlighted (using red boxes) in Figures 4.11 and 4.13.

	CNT(M)	CNT(M)	CNT(S)
Conductor	Undoped CNT	Aligned 1.0 iodine/u.c.	Interstitial 3.0 iodine/u.c.
		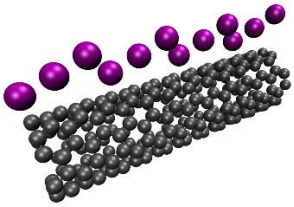	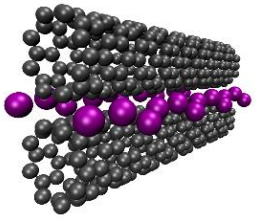
	$1/R_c = 2.00G_0$	$1/R_c = 2.08G_0$	$1/R_c = 3.00G_0$
	$\widehat{m}_c = 98.6\ amu/\text{Å}$	$\widehat{m}_c = 150.8 amu/\text{Å}$	$\widehat{m}_c = 275.5\ amu/\text{Å}$
Junction	Interstitial dopant	Interstitial dopant	Interstitial dopant
	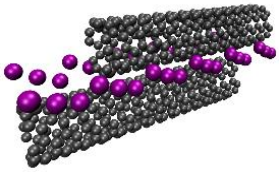	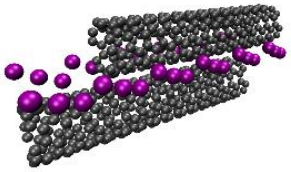	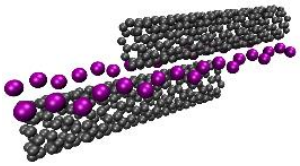
	$1/R_j = 1.52G_0$	$1/R_j = 1.52G_0$	$1/R_j = 1.83G_0$
	$m_j^{add} = 2538.1amu$	$m_j^{add} = 2538.1amu$	$m_j^{add} = 1395.9amu$

Table 5.2: High performance combinations of iodine doped CNT

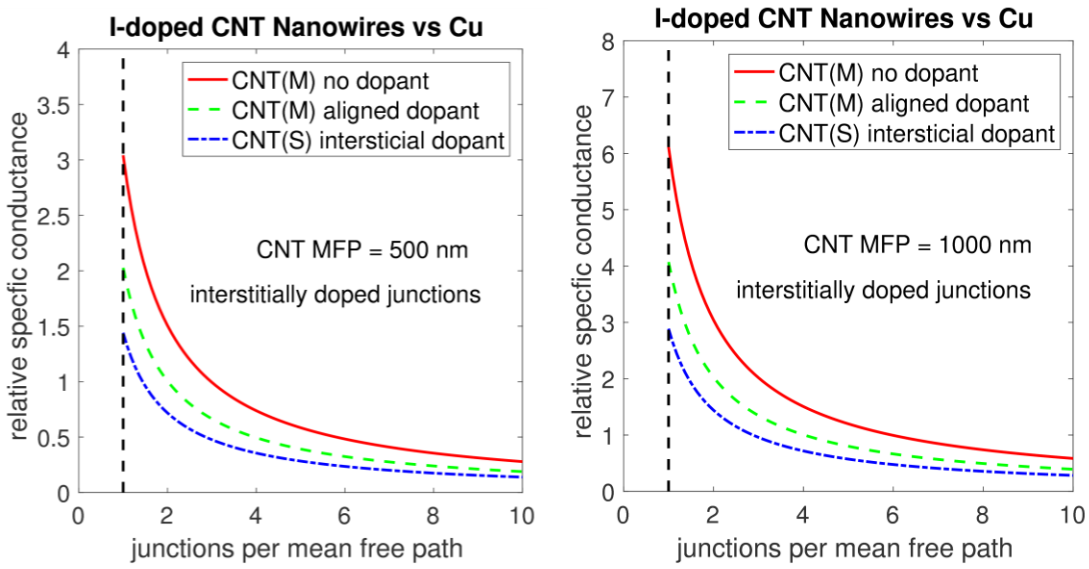

Figure 5.4: Performance evaluation on iodine doped CNT system

Figure 5.4 shows that when $\hat{n} = 1, L_{MFP} = 500nm$ the relative specific conductance M/M_{ref} of iodine doped CNT is around 1~3, which means that the performance of the CNT nanowire is one to three times better than that of copper, in terms of specific conductivity. This is consistent with published experimental results [3] on the performance of iodine doped CNT cables. This figure also suggests that the number of junctions per mean free path ($\hat{n}$) dominates the transmission line performance. The number of junctions in the cable should be limited in order to obtain high performance.

Chapter 6: Conclusions

In this chapter, general conclusions on the copper-CNT systems and polyiodide doped CNT systems analyzed in previous chapters will be discussed. In addition, the research contributions of the thesis will be summarized.

6.1 Double Wall Carbon and Copper Tubes

The analysis of Chapter 5 suggests a number of conclusions for the copper-CNT nanowires (the assumed mean free path is 50 nm):

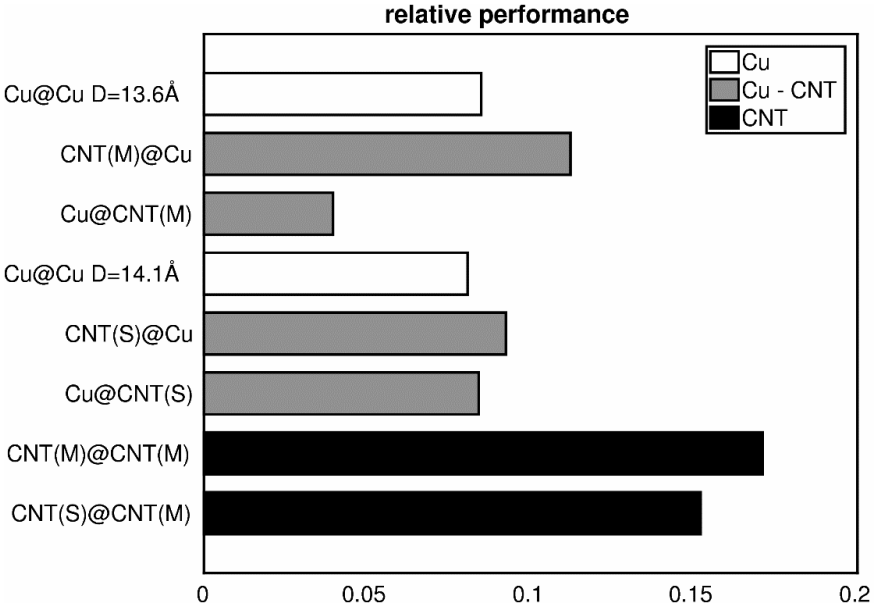

Figure 6.1: Relative performance of double wall tube systems (For copper-CNT $L_m = 50nm$, for CNT-CNT $L_m = 100nm$, for all $\hat{n} = 1$)

- In terms of specific conductivity, conventional copper wires are better, by an approximate factor of nine. Longer junction overlaps and different dopants may change this result
- The best configuration is CNT(M)@Cu

- The second best configuration is CNT(S)@Cu
- Improvements of the above two configurations on Cu@Cu are modest, as shown in Figure 6.1
- In the case of the Cu@CNT configurations, CNT(S) outperforms CNT(M) by an approximate factor of two

The analysis of Chapter 5 suggests a number of conclusions for the CNT-CNT nanowires (the assumed mean free path is 100 nm):

- In terms of specific conductivity, conventional copper wires are better, by an approximate factor of six. Longer junction overlaps and different dopants may change this result
- The best configuration is CNT(M)@CNT(M)
- The second best configuration is CNT(S)@CNT(M)
- The above two configurations improve on Cu@Cu by an approximate factor of two as shown in Figure 6.1
- In configurations with CNT(S) as the outside tube, the junctions are nearly open circuit

Overall, the Chapter 5 analyses of the dual wall (Cu-CNT and CNT-CNT) systems suggest several overarching conclusions:

- Although the doped junction conductance and double wall specific conductance calculations favor the copper-copper and copper-CNT configurations, at the nanowire level the CNT-CNT configurations appear to offer the most potential
- If the CNT mean free path is increased by an order of magnitude (to one micrometer), the predicted CNT-CNT nanowire performance exceeds that of conventional copper by more than seventy percent

- In all cases, the parasitic mass and resistance associated with 'excess' junctions significantly degrades nanowire performance
- The junction models considered here included minimal overlap and only chromium as a dopant; calculations with larger overlaps and different dopants are needed

6.2 Polyiodide Doped CNT

The analysis of Chapter 5 suggests a number of conclusions on polyiodide doped CNT nanowires:

- The analysis results are consistent with published experimental results [3], which indicate that iodine doped CNT conductors can offer specific conductivity in the range of one to three times that of copper
- The analyses considered smaller diameter nanotubes (by a factor of four) and higher dopant to carbon mass ratios (by a factor of three) than those described in published experiments [3], [17]
- Estimated CNT nanowire performance varies approximately linearly with CNT mean free path; published experimental data indicates that mean free path is reduced as temperature is increased [81]
- In the case of iodine doping, realizing high specific conductivity appears to require very mass efficient use of the dopant
- If significant charge transport does occur within the polyiodide, the latter conduction process may perhaps be due to a Grotthuss mechanism

6.3 Thesis Contributions

Over the course of the last two decades, considerable experimental research has investigated the ballistic conduction performance of SWCNT [25], MWCNT [35], doped CNT [3], [31], [82]–[84], CNT composites [85], [86], CNT junctions [49], and CNT

networks [79]. Complimentary computational research on these topics has also been performed [30]-[47], although the computational literature has been, by comparison, rather limited in scope, due in large part to the high computational cost of ab initio modeling. Given this substantial knowledge base, current experimental and computational research has shifted in focus, in order to address the development of macroscale carbon based conductors intended to replace copper in weight sensitive engineering applications. An example application is the development of high specific conductivity power and data cabling for civilian and military aircraft.

The contributions of this thesis, although fundamental in nature, reflect the aforementioned shift in experimental and computational research towards the engineering realization of new carbon based conductors, which may offer fundamental improvements on conventional copper cabling. The contributions are in three areas, all of which extend previous work in order to address problems associated with the design and manufacture of nanostructured conductors:

(1) the first contribution is a systematic analysis of ballistic conductance properties for random, aligned, and interstitial doping patterns in metallic and semiconducting CNT's and CNT junctions, for atomic iodine and polyiodide dopants; understanding the effects of such doping is of central importance in the development of carbon based conductors, since the large scale CNT arrays used to fabricate engineering cables are expected to include a diverse mix of metallic, semiconducting, single wall, and multiwall tubes incorporating a multitude of junctions and only coarsely aligned by the extrusion [87], gel spinning [17], or other processes used in macroscale manufacturing.

(2) the second contribution is a systematic analysis of the ballistic conductance properties of dual wall tube conductors, including metallic and semiconducting CNTs and CNT-copper nanocomposites; understanding the effects of multiwall structures on

conductor and junction performance is of central importance in the development of carbon based conductors, since: (a) as previously noted, multiwall configurations are the typical product of large scale CNT manufacturing processes, and (b) copper-CNT composites are at present the principal competitor [60] to 'pure' CNT systems in the development of high performance nanostructured cable systems.

(3) the third contribution is the development of a fully quantum based model of the specific conductivity of nanowires composed of doped CNT's, doped CNT junctions, and Cu-CNT composites; understanding the effects of mass density, added dopant mass, junction structure, component ballistic conductance, and electron mean free path on nanocomposite wiring is of central importance in the development of carbon based conductors, since such models are essential to: (a) estimating realistic performance goals in engineering development efforts, and (b) quantifying cost and performance tradeoffs associated with the pursuit of alternative nanoscale cable architectures.

The research completed in this thesis, and the corresponding experimental research literature, suggest many opportunities for future research. Of immediate interest are: (1) the modeling of more complex dopants, including ICl [84], $KAuBr_4$ [82], and others, (2) the modeling of multi-tube interactions (as computational costs permit), based on the experimentally observed complexity [88] of CNT cable architectures, and (3) the development of improved computational methods for both equilibrium calculations and ballistic conduction calculations, an essential enabler if computational research is to keep pace with experimental work on the increasingly complex cable nanostructures, doping systems, and fabrication processes of interest.

References

[1] M. F. L. De Volder, S. H. Tawfick, R. H. Baughman, and A. J. Hart, "Carbon nanotubes: present and future commercial applications.," *Science*, vol. 339, no. 6119, pp. 535–539, 2013.

[2] J. M. Wernik and S. a. Meguid, "Recent Developments in Multifunctional Nanocomposites Using Carbon Nanotubes," *Appl. Mech. Rev.*, vol. 63, no. 5, p. 50801, 2010.

[3] Y. Zhao, J. Wei, R. Vajtai, P. M. Ajayan, and E. V Barrera, "Iodine doped carbon nanotube cables exceeding specific electrical conductivity of metals.," *Sci. Rep.*, vol. 1, no. c, p. 83, 2011.

[4] C. Subramaniam, T. Yamada, K. Kobashi, A. Sekiguchi, D. N. Futaba, M. Yumura, and K. Hata, "One hundred fold increase in current carrying capacity in a carbon nanotube-copper composite.," *Nat. Commun.*, vol. 4, p. 2202, 2013.

[5] X. Wang, N. Behabtu, C. C. Young, D. E. Tsentalovich, M. Pasquali, and J. Kono, "High-ampacity power cables of tightly-packed and aligned carbon nanotubes," *Adv. Funct. Mater.*, vol. 24, no. 21, pp. 3241–3249, 2014.

[6] "Wikipedia - Carbon Nanotube." [Online]. Available: https://en.wikipedia.org/wiki/Carbon_nanotube.

[7] S. IIJIMA, "Helical microtubules of graphitic carbon," *Nature*, vol. 354, pp. 56–58, 1991.

[8] J. N. Coleman, U. Khan, W. J. Blau, and Y. K. Gun'ko, "Small but strong: A review of the mechanical properties of carbon nanotube-polymer composites," *Carbon*, vol. 44, no. 9. pp. 1624–1652, 2006.

[9] C. T. White and T. N. Todorov, "Carbon nanotubes as long ballistic conductors," *Nature*, vol. 393, no. 6682, pp. 240–242, 1998.

[10] S. Frank, P. Poncharal, Z. L. Wang, and W. A. de Heer, "Carbon nanotube quantum resistors," *Science*, vol. 280, no. 5370, pp. 1744–1746, 1998.

[11] A. Javey, J. Guo, Q. Wang, M. Lundstrom, and H. Dai, "Ballistic carbon nanotube field-effect transistors.," *Nature*, vol. 424, no. 6949, pp. 654–657, 2003.

[12] A. A. Balandin, "Thermal properties of graphene and nanostructured carbon materials.," *Nat. Mater.*, vol. 10, no. 8, p. 569, 2011.

[13] J. Che, T. Cagin, and W. A. Goddard III, "Thermal conductivity of carbon nanotubes," *Nanotechnology*, vol. 11, no. 2, p. 65, 2000.

[14] X. Lu and Z. Chen, "Curved Pi-conjugation, aromaticity, and the related chemistry of small fullerenes (<C60) and single-walled carbon nanotubes," *Chemical Reviews*, vol. 105, no. 10. pp. 3643–3696, 2005.

[15] X. Blase, L. X. Benedict, E. L. Shirley, and S. G. Louie, "Hybridization effects and metallicity in small radius carbon nanotubes," *Phys. Rev. Lett.*, vol. 72, no. 12, pp. 1878–1881, 1994.

[16] S. E. Harvey, "Carbon Conductor: A Pragmatic View," *Int. Wire Cable Connect. Symp.*, p. 558, 2012.

[17] N. Behabtu, C. C. Young, D. E. Tsentalovich, O. Kleinerman, X. Wang, A. W. K.

Ma, E. A. Bengio, R. F. ter Waarbeek, J. J. de Jong, R. E. Hoogerwerf, S. B. Fairchild, J. B. Ferguson, B. Maruyama, J. Kono, Y. Talmon, Y. Cohen, M. J. Otto, and M. Pasquali, "Strong, light, multifunctional fibers of carbon nanotubes with ultrahigh conductivity.," *Science*, vol. 339, no. 6116, pp. 182–186, 2013.

[18] J. N. Wang, X. G. Luo, T. Wu, and Y. Chen, "High-strength carbon nanotube fibre-like ribbon with high ductility and high electrical conductivity.," *Nat. Commun.*, vol. 5, no. 2005, p. 3848, 2014.

[19] J. M. Soler, E. Artacho, J. D. Gale, A. García, J. Junquera, P. Ordejón, and D. Sánchez-Portal, "The SIESTA method for ab initio order- N materials simulation," *J. Phys. Condens. Matter*, vol. 14, no. 11, p. 2745, 2002.

[20] S. Datta, "Nanoscale device modeling: the Green's function method," *Superlattices Microstruct.*, vol. 28, no. 4, pp. 253–278, 2000.

[21] K. Stokbro, J. Taylor, M. Brandbyge, and P. Ordejón, "TranSIESTA: A Spice for Molecular Electronics," in *Annals of the New York Academy of Sciences*, 2003, vol. 1006, pp. 212–226.

[22] J. Y. Park, S. Rosenblatt, Y. Yaish, V. Sazonova, H. Üstunel, S. Braig, T. A. Arias, P. W. Brouwer, and P. L. McEuen, "Electron-phonon scattering in metallic single-walled carbon nanotubes," *Nano Lett.*, vol. 4, no. 3, pp. 517–520, 2004.

[23] D. Mann, A. Javey, J. Kong, Q. Wang, and H. Dai, "Ballistic Transport in Metallic Nanotubes with Reliable Pd Ohmic Contacts," *Nano Lett.*, vol. 3, no. 11, pp. 1541–1544, 2003.

[24] Y. Imry and R. Landauer, "Conductance viewed as transmission," *Rev. Mod. Phys.*, vol. 71, no. 2, pp. S306–S312, 1999.

[25] J. Kong, E. Yenilmez, T. W. Tombler, W. Kim, H. Dai, R. B. Laughlin, L. Liu, C. S. Jayanthi, and S. Y. Wu, "Quantum interference and ballistic transmission in nanotube electron waveguides.," *Phys. Rev. Lett.*, vol. 87, no. 10, p. 106801, 2001.

[26] K. Stokbro, "First-principles modeling of electron transport.," *J. Phys. Condens. Matter*, vol. 20, no. 6, p. 64216, 2008.

[27] Z. Qian, R. Li, S. Hou, Z. Xue, and S. Sanvito, "An efficient nonequilibrium Green's function formalism combined with density functional theory approach for calculating electron transport properties of molecular devices with quasi-one-dimensional electrodes," *J. Chem. Phys.*, vol. 127, no. 19, 2007.

[28] R. Li, J. Zhang, S. Hou, Z. Qian, Z. Shen, X. Zhao, and Z. Xue, "A corrected NEGF + DFT approach for calculating electronic transport through molecular devices: Filling bound states and patching the non-equilibrium integration," *Chem. Phys.*, vol. 336, no. 2–3, pp. 127–135, 2007.

[29] B. Biel, F. J. Garcia-Vidal, A. Rubio, and F. Flores, "Ab initio study of transport properties in defected carbon nanotubes: an O(N) approach," *J. Phys. Condens. Matter*, vol. 20, no. 29, p. 15, 2008.

[30] H. Park, J. Zhao, and J. P. Lu, "Effects of sidewall functionalization on conducting properties of single wall carbon nanotubes," *Nano Lett.*, vol. 6, no. 5, pp. 916–919, 2006.

[31] D. Janas, K. Z. Milowska, P. Bristowe, and K. Koziol, "Improving the electrical

properties of carbon nanotubes with interhalogen compounds," *Nanoscale*, vol. 44, no. 27, pp. 3212–3221, 2017.
[32] S. Esconjauregui, L. D'Arsié, Y. Guo, J. Yang, H. Sugime, S. Caneva, C. Cepek, and J. Robertson, "Efficient Transfer Doping of Carbon Nanotube Forests by MoO3," *ACS Nano*, vol. 9, no. 10, pp. 10422–10430, 2015.
[33] K. K. Kim, J. J. Bae, H. K. Park, S. M. Kim, H.-Z. Geng, K. A. Park, H.-J. Shin, S.-M. Yoon, A. Benayad, J.-Y. Choi, and Y. H. Lee, "Fermi level engineering of single-walled carbon nanotubes by AuCl3 doping.," *J. Am. Chem. Soc.*, vol. 130, no. 38, pp. 12757–12761, 2008.
[34] R. Moradian, S. Azadi, and H. Refii-Tabar, "When double-wall carbon nanotubes can become metallic or semiconducting.," *J. Phys. Condens. Matter*, vol. 19, no. 17, p. 176209, 2007.
[35] M. Soto, T. A. Boyer, S. Biradar, L. Ge, R. Vajtai, A. Elías-Zúñiga, P. M. Ajayan, and E. V Barrera, "Effect of interwall interaction on the electronic structure of double-walled carbon nanotubes.," *Nanotechnology*, vol. 26, no. 16, p. 165201, 2015.
[36] X. J. Du, Z. Chen, J. Zhang, C. S. Yao, C. Chen, and X. L. Fan, "Structural and electronic properties of conducting Cu nanowire encapsulated in semiconducting zigzag carbon nanotubes: A first-principles study," *Phys. Status Solidi Basic Res.*, vol. 249, no. 5, pp. 1033–1038, 2012.
[37] T. Fujimori, A. Morelos-Gómez, Z. Zhu, H. Muramatsu, R. Futamura, K. Urita, M. Terrones, T. Hayashi, M. Endo, S. Young Hong, Y. Chul Choi, D. Tománek, and K. Kaneko, "Conducting linear chains of sulphur inside carbon nanotubes.," *Nat. Commun.*, vol. 4, p. 2162, 2013.
[38] A. Lopez-Bezanilla, "Electronic Transport Properties of Chemically Modified Double-Walled Carbon Nanotubes," *J. Phys. Chem. C*, vol. 117, pp. 15266–15271, 2013.
[39] C. Buia, A. Buldum, and J. P. Lu, "Quantum Interference Effects in Electronic Transport through Nanotube Contacts," *Phys. Rev. B*, vol. 67, no. January, pp. 113409–113412, 2003.
[40] F. Xu, A. Sadrzadeh, Z. Xu, and B. I. Yakobson, "Can carbon nanotube fibers achieve the ultimate conductivity? - Coupled-mode analysis for electron transport through the carbon nanotube contact," *J. Appl. Phys.*, vol. 114, no. 6, 2013.
[41] A. Buldum and J. P. Lu, "Contact resistance between carbon nanotubes," *Phys. Rev. B Condens. Matter*, vol. 63, no. 16, p. 161403(1-4), 2001.
[42] S. Ciraci, A. Buldum, and I. Batra, "Quantum effects in electrical and thermal transport through nanowires," *J. Phys. Condens.*, vol. 13, pp. 537–568, 2001.
[43] E. Y. Li and N. Marzari, "Improving the electrical conductivity of carbon nanotube networks: A first-principles study," *ACS Nano*, vol. 5, no. 12, pp. 9726–9736, 2011.
[44] K. H. Khoo and J. R. Chelikowsky, "Electron transport across carbon nanotube junctions decorated with Au nanoparticles: Density functional calculations," *Phys. Rev. B - Condens. Matter Mater. Phys.*, vol. 79, no. 20, p. 205422, 2009.

[45] D. J. Mowbray, C. Morgan, and K. S. Thygesen, “Influence of O2 and N2 on the conductivity of carbon nanotube networks,” *Phys. Rev. B - Condens. Matter Mater. Phys.*, vol. 79, no. 19, pp. 1–6, 2009.
[46] W. S. B. Meguid, S. A. Meguid, Z. H. Zhu, and M. J, “Modeling electrical conductivities of nanocomposites with aligned carbon nanotubes,” *Nanotechnology*, vol. 22, no. 48, p. 485704, 2011.
[47] S. Gong, Z. H. Zhu, and E. I. Haddad, “Modeling electrical conductivity of nanocomposites by considering carbon nanotube deformation at nanotube junctions,” *J. Appl. Phys.*, vol. 114, no. 7, p. 74303, 2013.
[48] Y. Li, D. Mann, M. Rolandi, W. Kim, A. Ural, S. Hung, A. Javey, J. Cao, D. Wang, E. Yenilmez, Q. Wang, J. F. Gibbons, Y. Nishi, and H. Dai, “Preferential Growth of Semiconducting Single-Walled Carbon Nanotubes by a Plasma Enhanced CVD Method,” *Nano Lett.*, vol. 4, no. 2, pp. 317–321, 2004.
[49] P. L. M. S. Fuhrer, J. Nygård, L. Shih, M. Forero, Young-Gui Yoon, M. S. C. Mazzoni, Hyoung Joon Choi, Jisoon Ihm, Steven G. Louie, A. Zettl, McEuen, “Crossed Nanotube Junctions,” *Science*, vol. 288, no. 5465, pp. 494–497, 2000.
[50] J. P. Perdew, K. Burke, and M. Ernzerhof, “Generalized Gradient Approximation Made Simple,” *Phys. Rev. Lett.*, vol. 77, no. 18, pp. 3865–3868, 1996.
[51] E. Artacho, E. Anglada, O. Diéguez, J. D. Gale, A. García, J. Junquera, R. M. Martin, P. Ordejón, J. M. Pruneda, D. Sánchez-Portal, and J. M. Soler, “The SIESTA method. developments and applicability.,” *J. Phys. Condens. Matter*, vol. 20, no. 6, p. 64208, 2008.
[52] J. D. Pack and H. J. Monkhorst, “Special points for Brillouin-zone integrations,” *Phys. Rev. B*, vol. 13, no. 4, pp. 5188–5192, 1976.
[53] G. Foti, “Elastic and inelastic electron transport through alkane-based molecular junctions,” CSIC-UPV - Centro de Física de Materiales (CFM), 2014.
[54] T. Frederiksen, “Inelastic transport theory for nanoscale systems,” Technical University of Denmark, 2007.
[55] J. X. Yu, Y. Cheng, S. Sanvito, and X. R. Chen, “Bias-dependent oscillatory electron transport of monatomic sulfur chains,” *Appl. Phys. Lett.*, vol. 100, no. 10, p. 103110, 2012.
[56] S. Liu, A. Nurbawono, and C. Zhang, “Density Functional Theory for Steady-State Nonequilibrium Molecular Junctions.,” *Sci. Rep.*, vol. 5, p. 15386, 2015.
[57] K. W. Jacobsen, J. T. Falkenberg, N. Papior, P. Bøggild, A. P. Jauho, and M. Brandbyge, “All-graphene edge contacts: Electrical resistance of graphene T-junctions,” *Carbon N. Y.*, vol. 101, pp. 101–106, 2016.
[58] A. Bachtold, M. S. Fuhrer, S. Plyasunov, M. Forero, E. H. Anderson, A. Zettl, and P. L. McEuen, “Scanned probe microscopy of electronic transport in carbon nanotubes.,” *Phys. Rev. Lett.*, vol. 84, no. 26, pp. 6082–5, 2000.
[59] K. S. Coleman, A. K. Chakraborty, S. R. Bailey, J. Sloan, and M. Alexander, “Iodination of single-walled carbon nanotubes,” *Chem. Mater.*, vol. 19, no. 5, pp. 1076–1081, 2007.
[60] D. F. Lee, M. Burwell, and H. Stillman, “Priority Research Areas to Accelerate the

Development of Practical Ultra-conductive Copper Conductors," 2015.
[61] G. Kiesiewicz, "Studies on obtaining Cu-CNT composites by continuous casting method," *Metall. Foundry Eng.*, vol. 40, no. 2, pp. 83–92, 2014.
[62] T. T. N. Banno, "Enhancement of electrical conductivity of Copper/CNT composite wire," *Japan Inst. Met.*, vol. 73–9, pp. 651–658, 2009.
[63] T. G. Holesinger, R. Depaula, J. Rowley, and K. Sperling, "Carbon Nanotube Composite Cables for Ultra-Deepwater Oil and Gas Fields," in *Offshore Technology Conference*, 2014, pp. 1–9.
[64] E. Artacho, J. D. Gale, A. Garc, J. Junquera, R. M. Martin, P. Ordej, and S. Daniel, "User' s Guide." 2015.
[65] C. Yang, "First Principle Studies of Cu-Carbon Nanotube Hybrid Structures with Emphasis on the Electronic Structures and the Transport Properties," University of Central Florida, 2013.
[66] M. Ghorbani-Asl, P. D. Bristowe, and K. Koziol, "A computational study of the quantum transport properties of a Cu-CNT composite," *Phys. Chem. Chem. Phys.*, vol. 17, no. 28, pp. 18273–18277, 2015.
[67] K. E. Moore, D. D. Tune, and B. S. Flavel, "Double-walled carbon nanotube processing," *Advanced Materials*, vol. 27, no. 20. pp. 3105–3137, 2015.
[68] K. Liu, C. Jin, X. Hong, J. Kim, A. Zettl, E. Wang, and F. Wang, "Van der Waals-coupled electronic states in incommensurate double-walled carbon nanotubes," *Nat. Phys.*, vol. 10, no. 10, pp. 737–742, 2014.
[69] Y. Baskin and L. Meyer, "Lattice constants of graphite at low temperatures," *Phys. Rev.*, vol. 100, no. 2, p. 544, 1955.
[70] Z. Wu, Y. Han, R. Huang, X. Chen, Y. Guo, Y. He, W. Li, Y. Cai, and N. Wang, "Semimetallic-to-metallic transition and mobility enhancement enabled by reversible iodine doping of graphene.," *Nanoscale*, vol. 6, no. 21, pp. 13196–202, 2014.
[71] X. Fan, E. Dickey, P. Eklund, K. Williams, L. Grigorian, R. Buczko, S. Pantelides, and S. Pennycook, "Atomic Arrangement of Iodine Atoms inside Single-Walled Carbon Nanotubes," *Phys. Rev. Lett.*, vol. 84, no. 20, pp. 4621–4624, 2000.
[72] L. Ci, Z. Rao, Z. Zhou, D. Tang, X. Yan, Y. Liang, D. Liu, H. Yuan, W. Zhou, G. Wang, W. Liu, and S. Xie, "Double wall carbon nanotubes promoted by sulfur in a floating iron catalyst CVD system," *Chem. Phys. Lett.*, vol. 359, no. 1–2, pp. 63–67, 2002.
[73] A. K. K. Rappé, C. J. J. Casewit, K. S. S. Colwell, W. A. Goddard III, and W. M. Skiff, "UFF, a Full Periodic Table Force Field for Molecular Mechanics and Molecular Dynamics Simulations," *J. Am. Chem. Soc.*, vol. 114, no. 25, pp. 10024–10035, 1992.
[74] C. D. E. Hanwell M.D. Lonie D.C., Vandermeersch, T., Zurek E., Hutchison, G., "Avogadro: An Advanced Semantic Chemical Editor, Visualisation, and Analysis Platform," *J. Chem. Informatics*, vol. 4.17, pp. 1–17, 2012.
[75] P. H. Svensson and L. Kloo, "Synthesis, structure, and bonding in polyiodide and metal iodide-iodine systems.," *Chem. Rev.*, vol. 103, no. 5, pp. 1649–84, 2003.

[76] I. Rubinstein and E. Gileadi, “Measurements of electrical conductivity in solid bromine and iodine,” *J. Electroanal. Chem.*, vol. 108, no. 2, pp. 191–201, 1980.
[77] Tatsuo Kaiho, *Iodine Chemistry and Applications*. John Wiley & Sons, Inc., 2014.
[78] B. R. Sankapal, K. Setyowati, J. Chen, and H. Liu, “Electrical properties of air-stable, iodine-doped carbon-nanotube-polymer composites,” *Appl. Phys. Lett.*, vol. 91, no. 17, pp. 10–13, 2007.
[79] P. N. Nirmalraj, P. E. Lyons, S. De, J. N. Coleman, and J. J. Boland, “Electrical connectivity in single-walled carbon nanotube networks,” *Nano Lett.*, vol. 9, no. 11, pp. 3890–3895, 2009.
[80] Y. Hanaoka, K. Hinode, K. Takeda, and D. Kodama, “Increase in Electrical Resistivity of Copper and Aluminum Fine Lines,” *Mater. Trans.*, vol. 43, no. 7, pp. 1621–1623, 2002.
[81] E. J. Fuller, D. Pan, B. L. Corso, O. T. Gul, and P. G. Collins, “Mean free paths in single-walled carbon nanotubes measured by Kelvin probe force microscopy,” *Phys. Rev. B*, vol. 89, no. 24, p. 245450, 2014.
[82] J. Alvarenga, P. R. Jarosz, C. M. Schauerman, B. T. Moses, B. J. Landi, C. D. Cress, and R. P. Raffaelle, “High conductivity carbon nanotube wires from radial densification and ionic doping,” *Appl. Phys. Lett.*, vol. 97, no. 18, pp. 19–22, 2010.
[83] I. Puchades, C. C. Lawlor, C. M. Schauerman, A. R. Bucossi, J. E. Rossi, N. D. Cox, and B. J. Landi, “Mechanism of chemical doping in electronic-type-separated single wall carbon nanotubes towards high electrical conductivity,” *J. Mater. Chem. C*, vol. 3, no. 39, pp. 10256–10266, 2015.
[84] D. Janas, A. P. Herman, S. Boncel, and K. K. K. Koziol, “Iodine monochloride as a powerful enhancer of electrical conductivity of carbon nanotube wires,” *Carbon N. Y.*, vol. 73, no. February 2014, pp. 225–233, 2014.
[85] L. Fan and X. Xu, “A stable iodine-doped multi-walled carbon nanotube-polypyrrole composite with improved electrical property,” *Compos. Sci. Technol.*, vol. 118, pp. 264–268, 2015.
[86] J. T. Wescott, P. Kung, and A. Maiti, “Conductivity of carbon nanotube polymer composites,” *Appl. Phys. Lett.*, vol. 90, no. 3, p. 33116, 2007.
[87] S. Ata, H. Yoon, C. Subramaniam, T. Mizuno, A. Nishizawa, and K. Hata, “Scalable, solvent-less de-bundling of single-wall carbon nanotube into elastomers for high conductive functionality,” *Polym.*, vol. 55, no. 20, pp. 5276–5283, 2014.
[88] T. Wang, X. Hu, and S. Dong, “Construction of metal nanoparticle/multiwalled carbon nanotube hybrid nanostructures providing the most accessible reaction sites,” *J. Mater. Chem.*, vol. 17, no. 39, pp. 4189–4195, 2007.